ORIGINAL ARTICLE

Preparation of nano zero-valent aluminum for one-step removal of methylene blue from aqueous solutions: cost analysis for scaling-up and artificial intelligence

Ahmed H. Sadek[1,2] · Mohamed K. Mostafa[3]

Abstract

Methylene blue (MB) is a heterocyclic aromatic dye that is difficult to biodegrade due to its complex chemical structure. In this study, chemically prepared nano zero-valent aluminum (nZVAl) was investigated for the first time for one-step removal of MB from aqueous solutions under different experimental factors (pH, dosage, time, MB concentration, stirring rate, temperature, detergents, and ionic strength). The prepared nZVAl material was characterized using XRD, TEM, SEM, EDS, and FTIR. Results indicated that at an initial MB concentration of 10 mg/L, pH 10, nZVAl dosage 1.0 g/L, stirring rate 200 rpm, and temperature 30 °C, the removal efficiency of approximately 99.0% was achieved within an equilibrium time of 90 min. An improvement in MB removal efficiency was observed in the presence of inorganic salts, while the presence of detergents resulted in a reduction in MB removal efficiency. The isotherm adsorption data were best fitted by the Freundlich isotherm model (R^2: 0.9569), while the kinetic data were well described by the pseudo-second-order (PSO) model (R^2: 0.9999). Based on the thermodynamic study, the MB adsorption process is physically diffusion-controlled. The adsorption of MB onto nZVAl was accurately described using an artificial neural network (ANN) with a structure of 11–10–1 and R^2 of 0.97. The overall cost of scaling up the adsorption unit to be used for MB removal from aqueous solutions under the optimum conditions is about US\$1.31/m^3. Consequently, this study opens the door for other researchers to test nZVAl in treating real textile wastewater.

Keywords Adsorption mechanisms · Aluminum nanoparticles · Artificial neural network · Cost analysis and scaling-up · Methylene blue · Thermodynamic

Introduction

Despite the textile industry representing 7% of the total global exports, this sector is one of the major polluters worldwide (Lellis et al. 2019). Textile industries release a huge amount of colored/highly toxic wastewater due to utilizing different types of synthetic dyes during the dyeing process, such as methylene blue (MB) (Hamdy et al. 2018). MB is a cationic dye that has a complex chemical structure (molecular formula: $C_{16}H_{18}N_3SCl$), which makes it stable and difficult to be biodegraded (Hamdy et al. 2019a, b). It has been estimated that the MB concentration in dyes used by the textile industry is normally about 50 mg/L (Hamdy et al. 2019a, b). MB discharged from textile and dye manufacturing industries can cause serious health issues, including vomiting, eye damage, nausea, skin irritation, diarrhea, dyspnea, convulsions, upset stomach, tachycardia, cyanosis, as well as deterioration of the central nervous system, kidneys, liver, and brain (Arabi and Sohrabi 2014; Kavitha and Namasivayam 2007; Li et al. 2013a, b; Li et al. 2013a, b). In addition, water bodies contaminated with MB may suffer from a lack of sunlight penetrating water, which may affect the entire aquatic ecosystem by reducing photosynthetic function and dissolved oxygen levels (Hassan and Carr 2018; Imran et al. 2015; Lellis et al. 2019). Therefore, water

✉ Ahmed H. Sadek
ahsadek@zewailcity.edu.eg

✉ Mohamed K. Mostafa
m_khaled@buc.edu.eg

1   Environmental Engineering Program, Zewail City of Science, Technology and Innovation, 6th October City, Giza 12578, Egypt

2   Sanitary and Environmental Engineering Research Institute, Housing and Building National Research Center (HBRC), Dokki, Giza 11511, Egypt

3   Faculty of Engineering and Technology, Badr University in Cairo (BUC), Greater Cairo 11829, Egypt

contaminated with MB must be sufficiently treated before reaching surface water bodies.

The common methods used for MB removal from aqueous solutions include coagulation and flocculation, biological treatment, membrane filtration, electrochemical treatment, and adsorption processes (Chen et al. 2016; Mostafa et al. 2021, 2017; Raman and Kanmani 2016). The coagulation and flocculation processes involve serious disposal problems, where large quantities of sludge and by-products are generated (Hamdy et al. 2018). Electrochemical treatment is very effective in dye removal; however, it consumes large amounts of energy and needs special equipment (Mahmoud et al. 2021c). In addition, strict controls over pH and temperature are required in the case of applying biological treatment methods (Chao et al. 2017). The main drawback of applying the membrane filtration technique is concentrated sludge production (Foo and Hameed 2012). Currently, the adsorption treatment technique has grabbed the attention of many researchers due to its simple design, high efficiency, low capital and operation costs, ease of operation, and the possibility of regenerating and reusing the adsorbent (Alqadami et al. 2016; Bao and Zhang 2012; Daneshvar et al. 2017; Hu et al. 2011). The adsorption process is normally conducted in four consecutive phases (Aljeboree et al. 2017; Karthikeyan et al. 2005; Önal et al. 2006): (1) the adsorbate molecules travel from the liquid medium to the external film surrounding the adsorbent material; (2) the adsorbate molecules accumulated on the external film then move across the liquid film until reaching the exterior sites on the surface of the adsorbent; (3) the adsorbate molecules migrate within the voids of the adsorbent through intraparticle diffusion; and (4) the adsorbate binds to the internal adsorptive sites.

Sorbent materials can be obtained from numerous sources, such as industrial-derived products (Hamdy et al. 2019a, b), agricultural wastes (Mahmoud et al. 2021b), carbonaceous-based materials (Senthilkumaar et al. 2005), and woody biomass (Gouamid et al. 2013). The commonly used adsorbent materials include wheat shells, algal strains, date palm leaves, activated carbon (AC), coir pith carbon, graphene oxide, activated bentonite, tamarind fruit shells, masau stones, Ephedra strobilacea sawdust, carbon nanotubes, and activated lignin-chitosan pellets (Li et al. 2013a, b; Mahmoud 2022). Recently, nanoscale-based materials have proven to be efficient and reliable in the removal of dye compounds from contaminated water (Elshayb et al. 2022; Satapanajaru et al. 2011). The main advantages of nanomaterials over other adsorbents include high porosity, low production cost (Oprčkal et al. 2017; Shih et al. 2011; Wang et al. 2014), as well as small particle size (diameter range from 50 to 100 nm), which increases the surface area and thus allows more adsorbent molecules to come into contact with the porous phase (El-Shafei et al. 2016; Mahmoud et al. 2021a; Wang et al. 2021). Due to its high reactivity,

nano zero-valent aluminum (nZVAl) has received great attention in recent years in the field of wastewater treatment (Nidheesh et al. 2018). The ZVAl is not only a powerful adsorbent but also has a strong reductive capacity (Deng et al. 2020). Equation (1) demonstrates that under ambient conditions, nZVAl is an effective electron donor (Ileri and Dogu 2022; Xie et al. 2020).

$$Al^0 \rightarrow Al^{3+} + 3e^- \left(E^0 = -1.662V \right) \tag{1}$$
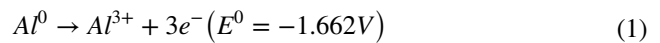
Recently, researchers have reported that ZVAl may be capable of eliminating non-biodegradable pollutants by generating sulfate and hydroxyl radicals in a water medium (Ileri and Dogu 2022). Nano zero-valent aluminum has been successfully employed in the treatment of water contaminated with dye compounds, chloride, bisphenol A, chromium(VI), phenol, nitrate, nitrobenzene, hexabromocyclododecane, and perchlorate (Ileri and Dogu 2022).

Prediction using an artificial neural network (ANN) has become an essential step in the wastewater treatment sector for the purpose of reducing treatment costs through process optimization. ANN can obtain relationships between inaccurate data by creating a link between input variables against each other and with output values (Mahmoud et al. 2020; Mahmoud and Mahmoud 2021; SaryEl-deen et al. 2017). Ratnam et al. (2022) forecasted MB removal from aqueous solutions using ANN and a UV-irradiated nano-graphene oxide (UV/n-GO). They have reported that the ANN was accurate in describing MB adsorption onto UV/n-GO with $R^2 = 0.92$. Amor et al. (2021) predicted MB removal by titanium dioxide (TiO$_2$) nanoparticles using ANN. The authors have also confirmed the accuracy of ANN in describing MB adsorption onto TiO$_2$ nanoparticles with $R^2 = 0.996$. In another study, Hamdy et al. (2019a, b) have conducted a comparison between using ANN and Response Surface Methodology (RSM) in predicting the adsorption of MB onto nano zero-valent iron (nZVI). They have reported that the ANN with $R^2 = 0.9313$ was more accurate than the RSM with $R^2 = 0.6316$ in describing MB adsorption onto nZVI. Mohammadzadeh Kakhki et al. (2020) have also reported a high R^2 value of 0.92 when applying ANN in describing MB adsorption onto sulfur–nitrogen co-doped Fe$_2$O$_3$ nanostructure.

To the best of our knowledge, there is no research in the literature regarding cationic dyes (such as MB) adsorption from contaminated water using nZVAl. The mineralogical, chemical, as well as physical properties of the prepared nZVAl were identified using X-ray diffraction (XRD), scanning electron microscopy (SEM), energy-dispersive spectroscopy (EDS), transmission electron microscope (TEM), and Fourier transform infrared (FTIR). This study aims to investigate MB removal from aqueous solutions using nZVAl under different environmental factors (pH, nZVAl

dosage, initial MB concentration, contact time, stirring rate, temperature, detergents, and ionic strength). Isotherms, kinetics, and thermodynamic models were used to fit the adsorption data. The adsorption performance was also predicted using an artificial neural network (ANN) tool. ANN was used to obtain the correlation between the MB removal efficiency and the studied environmental factors. The capital expenditures (CAPEX) and operating expenses (OPEX) of scaling up the treatment unit were also estimated.

Materials and methods

Preparation of methylene blue solution

MB was obtained from Farbwerke Hoechst AG Company, Germany. One gram of MB powder was dissolved in 1,000 mL of Milli-Q distilled water to prepare a stock solution of MB (1000 mg/L). The desired concentrations of 10, 20, 30, 40, 50, 60, 70, and 80 mg/L were then obtained by successive dilutions of the solution. The pH adjustment was conducted using sodium hydroxide solution (0.1 mol/l, NaOH) purchased from Honeywell Fluka Company, Germany, or hydrochloric acid solution (0.1 mol/l, HCl) purchased from SDFCL Sd Fine Chem Limited Company, India.

Preparation of nZVAl

Zero-valent aluminum nanoparticles were prepared by reducing aluminum ions using sodium borohydride (NaBH$_4$, powder, $\geq 98.0\%$, Winlab Co., UK). Precisely, the zero-valent aluminum nanoparticles were prepared in a 250 mL Erlenmeyer flask by dissolving aluminum sulfate (Al$_2$(SO$_4$)$_3$.18H$_2$O, 98%, AR, Loba Chemie, India) in distilled water, and the solution was stirred vigorously using a magnetic stirrer at 500 rpm. To reduce aluminum ions to zero valence aluminum nanoparticles, a burette was used to add 25 mL of the aqueous borohydride solution dropwise to 25 mL of the aqueous solution of aluminum ions (Al^{3+}). The pH increased from pH 2 to pH 5 at the end of the reaction, accompanied by fizz due to the elevation of the produced hydrogen gas. In the meantime, the temperature of the reaction increased while adding the reducing agent to the aluminum ion solution. All experiments were performed at a temperature of 25 °C. The reaction could be expressed by Eq. (2).

$$2Al^{3+} + 6BH_4^- + 18H_2O \rightarrow 2Al^0 + 6H_2BO_3^- + 24H^+ + 12H_2$$
(2)
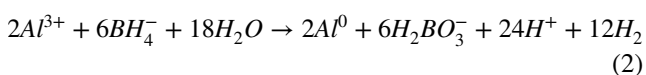
The mixture was stirred for an additional 20 min after the end of the reaction to ensure the complete reaction between the reducing agent and the dissolved aluminum ions, and

also to complete the growth and shape of the precipitated nZVAI nanoparticles. Afterward, the produced zero-valent aluminum nanoparticles were collected from the reaction medium by vacuum filtration. Then the nZVAI nanoparticles were washed with a large amount of distilled water and finally washed 3 times with ethyl alcohol before being dried in a drying oven at 110 °C for 6–8 h. For storage, a thin layer of ethyl alcohol was added to the surface of the prepared nZVAI nanoparticles, which is sufficient to preserve the nZVAI nanoparticles against further oxidation.

Equipment

An ultraviolet–visible spectrophotometer (T70 + UV/VIS Spectrometer, PG Instruments Ltd., UK) fitted with a quartz cell with a 1.0 cm path length was used to measure the concentrations of MB. The samples, after being removed from batch experiments, were filtrated using Whatman membrane filters with a 0.2 μm pore size. A maximum absorbance (λ_{max}) at 670 nm was determined to find the concentrations of MB in the filtrate solutions. The X-ray powder diffraction (XRD, Panalytical X'Pert Pro Multipurpose Diffractometer, Netherlands) was used to analyze the nZVAl nanoparticles. The equipment was provided by CuKα radiation with a wavelength of 1.54 Å. The crystallite size of nZVAl nanoparticles was determined using the Scherrer equation (Eq. (3)) (Sadek et al. 2021).

$$D = \frac{K\lambda}{\beta \cos\theta}$$
(3)

where D is crystallite size, K is the crystallite shape factor, λ is the X-ray wavelength, β is the full width at half maximum (FWHM), and θ is the diffraction angle.

The High-Resolution Transmission Electron Microscope (HR-TEM, JEM-2100, Japan) was used to study the morphology of nZVAl nanoparticles at a magnification of 25 kX and a voltage of 200 kV. A Field Emission Scanning Electron Microscope (FE-SEM, Philips, Quanta FEG 250, USA) equipped with an energy-dispersive spectrometer (EDS) was used to disclose the surface structure and chemical composition of the nZVAl nanoparticles before and after the adsorption process of MB at a magnification of 16 kX and a voltage of 20 kV. Fourier transform infrared spectroscopy (FTIR, JASCO FT/IR-6100A, Japan) measurements were conducted with KBr pellets to recognize the infrared spectra of the nZVAl adsorbent before and after MB adsorption in the range of 4000–450 cm^{-1}.

Batch experiments

Batch experiments in Erlenmeyer flasks with a volume of 250 mL were conducted to investigate the adsorption of MB

onto nZVAl. A one-factor at-a-time technique was used to examine the effects of different environmental conditions on MB removal efficiency, viz., pH values (2–12), nZVAl dosage (0.1–1.0 g/L), MB concentrations (10–80 mg/L), stirring rates (100–300 rpm), adsorption temperatures (30–60 °C), detergents (liquid Vanish granules and liquid Ariel: 0.1, 0.5, and 5 g), and ionic strength (sodium sulfate (Na_2SO_4): 2.10 M to 8.43 M, sodium chloride (NaCl): 1.72 M to 6.88 M, and sodium carbonate (Na_2CO_3): 2.82 M to 11.31 M. The studied factors and the range of the experiment for each factor were chosen based on the literature (Hamdy et al. 2018, 2019a, b). All experiments were conducted in triplicate. Equation (4) was used for calculating MB removal efficiency.

$$R(\%) = \frac{C_o - C_f}{C_o} \times 100 \tag{4}$$

where R is the removal efficiency of MB (%), C_o is the initial MB concentration (mg/L), and C_f is the final MB concentration (mg/L).

Equation (5) was used to estimate the MB adsorption capacity onto nZVAl.

$$q = \frac{(C_o - C_f)xV}{W} \tag{5}$$

where q is the quantity of MB adsorbed per unit mass of nZVAl (mg/g), V is the solution volume (L), and W is the nZVAl mass (g).

Design of an artificial neural network

Neural network structure

Figure 1 shows an artificial neural network (ANN) which was expressed as 11–10–1 and was configured with input, hidden, and output layers to predict the MB removal efficiency. The input layer received data from eleven experimental factors, i.e., residence time, initial MB concentration, temperature, pH, stirring rate, nZVI dosage, the concentration of two detergents: Ariel and Vanish, and the concentration of three salts: NaCl, Na_2CO_3, and Na_2SO_4. The hidden layer is made up of 10 neurons, where the optimum numbers
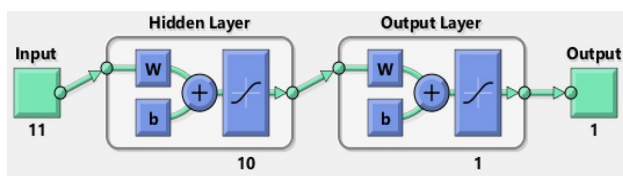

Fig. 1 ANN of 11–10–1 structure used for the prediction of MB removal efficiency by nZVAl

of neurons were projected by a trial-and-error method. The output layer represents the MB removal efficiency. The target and input vectors were categorized into three subgroups (Mahmoud et al. 2021c, 2017b): 60% for training, where the mean squared error (MSE) is minimized by adjusting the weights and biases of the neural network; 20% for validation to terminate the training step early and thus avoid data overfitting; and 20% for testing the efficiency and validity of the created ANN model (Elshfai et al. 2022).

ANN properties

In this study, the data were classified by applying a feedforward backpropagation algorithm (Mahmoud et al. 2018b). The "tansig" transfer function (Eq. (6)) and the "purlin" activation function (Eq. (7)) were chosen for the hidden and output layers, respectively. The mean squared error (MSE) (Eq. (8)) was used for two main purposes: (1) to compare both the output and the target data; and (2) to adjust the weights and the biases. Since the network applied in this research is located in the category of small and medium-sized networks, the Levenberg–Marquardt method (trainlm) was used for the training step (Mahmoud et al. 2017a; SaryEl-deen et al. 2017).

$$f(x) = x, -\infty < f(x) < +\infty \tag{6}$$

$$f(x) = \frac{e^x - e^{-x}}{e^x + e^{-x}}, -1 \leq f(x) \leq 1 \tag{7}$$

$$MSE = \frac{\sum_{i=1}^{N} (t_i - a_i)^2}{N} \tag{8}$$

where a_i is the predicted output, t_i is the predicted target, and N is the number of measured data.

Results and discussion

Characterization of nZVAl

The XRD pattern of the nZVAI particles with various peak intensities is displayed in Fig. 2a. The Al (111), Al (200), Al (220), and Al (311) planes of the α-Al^0 face-centered cubic cell phase were indicated by the high peaks at 38.43°, 44.60°, 64.88° and 78.09°, respectively. These findings prove the existence of aluminum nanoparticles in their zero-valent state (Al^0). Some other undesirable peaks have been observed in the range of $2\theta = 20°$–$35°$, which may be due to the presence of impurities formed during the reaction, such as the sodium sulfate salt (Na_2SO_4). The Na_2SO_4 was not completely eliminated during washing the precipitate, as sodium borohydride contributes to

Element	Weight %	Atomic %	Net Int.	Net Int. Error
C K	29.54	40.51	10.7	0.02
O K	39.3	40.47	39.2	0.01
AlK	31.16	19.03	163.2	0

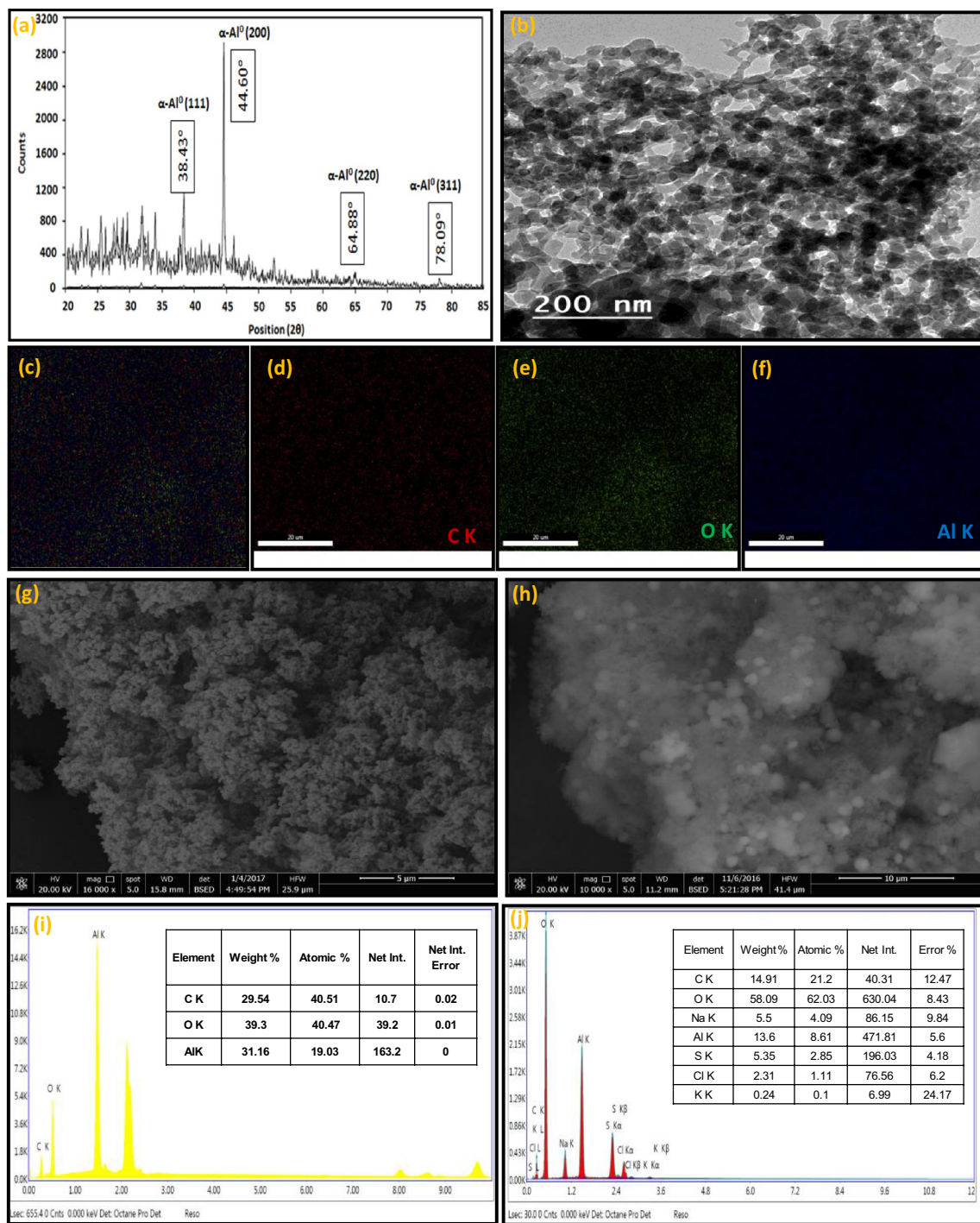| Element	Weight %	Atomic %	Net Int.	Error %
C K	14.91	21.2	40.31	12.47
O K	58.09	62.03	630.04	8.43
Na K	5.5	4.09	86.15	9.84
Al K	13.6	8.61	471.81	5.6
S K	5.35	2.85	196.03	4.18
Cl K	2.31	1.11	76.56	6.2
K K	0.24	0.1	6.99	24.17

Fig. 2 Characterization of nZVAl by **a** XRD, **b** TEM, **c–f** EDS elemental mapping, **g** SEM image before MB adsorption, **h** SEM image after MB adsorption, **i** EDS spectrum (inset: Table of chemical composition) before MB adsorption, and **j** EDS spectrum (inset: Table of chemical composition) after MB adsorption

the sodium ion, while the sulfate ion comes from the aluminum sulfate salt. Therefore, several washing processes with different solvents are required to diminish these impurities. In addition to the possibility that a small percentage of aluminum metal was partially oxidized during the preparation and washing process, we expect that the prepared aluminum particles are Al^0 aluminum core with an outer oxide shell mostly of amorphous Al_2O_3 which acts as an inert layer to protect the aluminum from further oxidation (Smith et al. 2017).

By the visual observation of the TEM image (Fig. 2b) of nZVAl particles, it could be observed that the particles are semi-spherical, and the majority of the nanoparticles range in size less than 100 nm. Moreover, previous studies reported that the aluminum oxide might represent the outer thin layer (a shell), and Al^0 was the core of the nanoparticles (Nidheesh et al. 2018; Peng et al. 2022). Additionally, some irregularly grouped nanoparticles with different sizes and shapes formed significant nanoclusters and showed nanoparticle agglomerates consisting of primary nanoparticles (Lozhkomoev et al. 2020). These findings might be attributed to the coupling of surface plasmons, excitons, dipole–dipole interactions, and the large surface area of the individual particles (Huang et al. 2020).

Furthermore, the primary components of this core–shell structure were characterized using EDS electronic mapping (Fig. 2c–f). According to experimental findings, the nZVAl nanoparticles contain the primary constituents of Al, O, and C. It is evident that the maps of the distribution of the Al and O elements, with weights% of 31.16 wt.% and 39.3 wt.%, respectively, have the same symmetry and density. Otherwise, the element map of C showed a similar symmetry but with a lower density and more evenly spaced particle distributions, with a weight% of 29.54 wt.%. These results provide additional evidence that the nZVAl nanoparticles have been successfully formed since the inter-particle distributions of the Al and O elements are more intense than those for the C element, and the nZVAl nanoparticles have been coated by a thin layer of Al$_2$O$_3$ as a shell.

The SEM of the synthesized nZVAl nanoparticles before adsorption is shown in Fig. 2g. As can be observed, the nanoparticles formed an uneven surface structure with lots of irregular and noncircular pores. Furthermore, some nanoparticles are gathered to form bigger nanoclusters, whereas the primary reasons for the chain-like and agglomerated structures of various particles with sizes less than 100 nm are due to the surface tension and electrostatic interaction with a true metal–metal inter-crystalline boundary. Similar chain-like aggregates have already been seen in prior work by El-khatib et al. (2021).

After the MB adsorption, some morphological alterations were observed when the MB solution encountered the nZVAl surface (see Fig. 2h). It was noted that the pores vanished, where the dye molecules filled in the open spaces and organized into a variety of different sizes and shapes of aggregates. This demonstrated that some MB molecules formed an adsorbate layer covering the surface of nZVAl, while others were adsorbed inside the inner pores of the nZVAl indicating the great affinity of the nZVAl nanoparticles for adsorption of MB dye.

The chemical composition of nZVAl nanoparticles before and after MB adsorption was examined using the EDS spectra (Fig. 2i, j). The presence of C and O elements

was attributed to the use of ethanol during washing and/or the partial oxidation of nZVAl during sample preparation and transfer. In terms of weight%, nZVAl contained 31.16 percent aluminum. According to Sahu et al. (2014), the existence of a sharp peak of Al at 1.5 keV is related to the elemental aluminum and indicates that the major content of the obtained sample consists of an aluminum element. According to the EDS findings, the oxygen content in the produced nZVAl nanoparticles appears to be relatively lower than the aluminum content. The undefined high-intense peaks at 2.2 keV and other peaks at 8, 8.5, and 9.7 keV refer to the gold substrate that is used for the ultra-thin coating of the nZVAl sample during the measurement process. The elemental profile of the EDS after MB adsorption revealed that MB dye successfully adsorbed to the nZVAl surface, as evidenced by the development of peaks of S, Na, Cl, and K elements. In addition, it could be observed that the weight% of Al decreased from 31.16 wt.% (before MB adsorption) to 13.6 wt.% (after MB adsorption), and the weight% of O increased from 39.3 wt.% (before MB adsorption) to 58 wt.% (after MB adsorption), respectively, indicating the further oxidation of nZVAl particles and the formation of a thicker shell of Al$_2$O$_3$ layers during the adsorption process.

The FTIR spectra of pure MB between 4000 and 450 cm^{-1} (Fig. 3) show the functional groups linked with the MB absorption peaks, which are –NH/–OH overlapped stretching vibration at 3445 cm^{-1} and CH $=$ N stretching amide II at 1638 cm^{-1}, respectively. The other MB absorption peaks include C–N at 1153 cm^{-1} and C–H out-of-plane bending vibrations of the ring at 611 cm^{-1}, respectively (Alshehri and Malik 2019; Xia et al. 2019). The functional groups of nZVAl before and after MB adsorption were recorded within the infrared spectra ranging between 4000 and 450 cm^{-1} as shown in Fig. 3. The
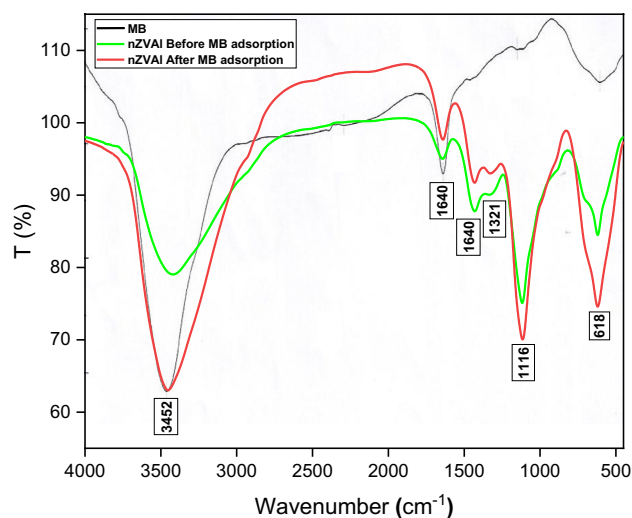

Fig. 3 IR spectra of MB and nZVAl before/after MB adsorption

sorption of MB inside the pores and on the surface of nZVAl may be the reason for the decrease in peak intensities. Certain peaks also underwent peak shifting after MB adsorption. The contribution of O–H and N–H stretching vibrations was demonstrated by the broad peaks at 3420 cm^{-1} shifted to 3452 cm^{-1}. Additionally, a peak was originally at 1640 cm^{-1} due to the attraction of some water molecules on the surface of the nZVAl particles. The aromatic ring exhibited a C=C and C–C asymmetric stretching at 1431 and 1321 bands, respectively. Generally, the peak at 1116 cm^{-1} is attributed to the C–O stretch of alcohols, carboxylic acids, and esters where the peak at 618 cm^{-1} mostly refers to Al–O bonding. These findings suggest that the adsorption of MB might be attributed to

several functional groups, including C–H, C=C, C–C, and C–O bonds (González-Gómez et al. 2019).

Effects of operating parameters

Effect of pH

The pH of the solution has a significant impact on the oxidation and the adsorption processes since it controls both the attraction force of the MB molecules and the surface binding sites (SBSs) on the nZVAl particle (Ileri and Dogu 2022). The removal efficiencies of MB at different pH values (2–12) are presented in Fig. 4a. For each pH value, all experimental factors were kept constant at an initial MB concentration of
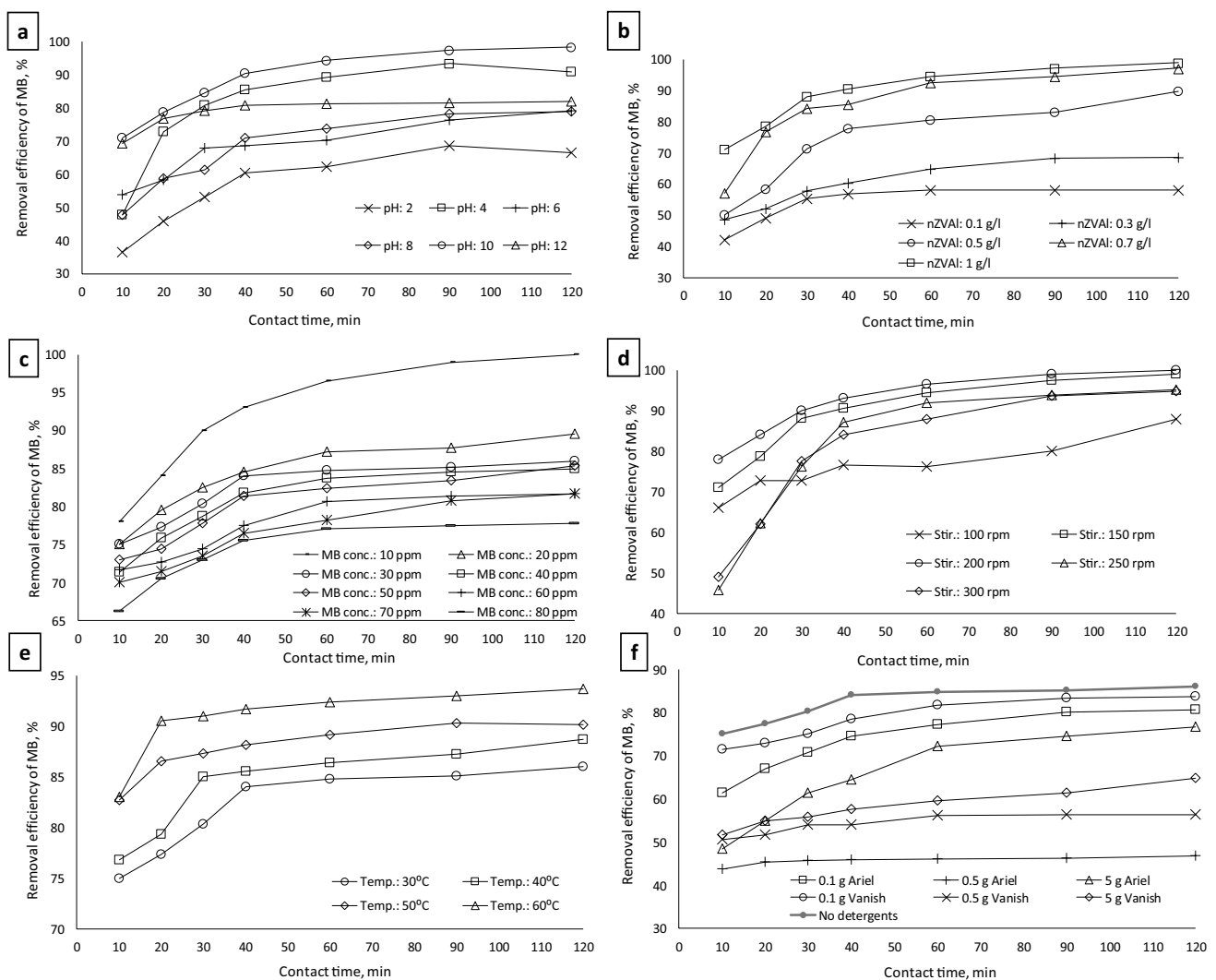
Fig. 4 Effects of operating parameters on the removal efficiency of MB by nZVAl **a** initial pH at $C_o = 10$ mg/L, stirring rate 150 rpm, nZVAl dosage 0.5 g/L, and temperature 30 °C, **b** nZVAl dosage at pH 10, $C_o = 10$ mg/L, stirring rate 150 rpm, and temperature 30 °C, **c** C_o at pH 10, nZVAl dosage 1.0 g/L, stirring rate 200 rpm, and temperature 30 °C, **d** stirring rate at pH 10, nZVAl dosage 1.0 g/L, $C_o = 10$ mg/L, and temperature 30 °C, **e** temperature at pH 10, nZVAl dosage 1.0 g/L, $C_o = 30$ mg/L, and stirring rate 200 rpm, **f** adding detergents at $C_o = 30$ mg/L, pH 10, stirring rate 200 rpm, nZVAl dosage 1.0 g/L, and temperature 30 °C

10 mg/L, stirring rate of 150 rpm, nZVAl dosage of 0.5 g/L, and temperature of 30 °C, except residence time which varied from 10 to 120 min. In the acidic media (pH 2–6), the surface of aluminum nanoparticles was positively charged due to the excess hydronium ions (H^+) in the solution. Thus, the MB cationic dye was difficult to be adsorbed as a result of the electrostatic repulsion (Saha 2010). There is also a high chance that the metal dissolves or separates at low pH values, thus reducing its adsorption capacity. The removal efficiency of MB improved as pH increased, especially in the alkaline media (pH ˃ 6). This is mainly due to the formation of aluminum hydroxide ($Al(OH)_3$) and aluminum oxide (Al_2O_3) on the surface of the nZVAl which enhances the electron transfer between MB dye and the surface of the nZVAl (Hu et al. 2011). Gulicovski et al. (2008) have reported that the point of zero charge (PZC) for various aluminum hydroxides and oxides varies widely from 5 to 9.6. For this reason, the highest MB removal efficiency was reported in the alkaline media at pH 10 ($pH_{solution} > pH_{PZC}$), where complexes were formed between the MB cationic dye and the negative charge on the nZVAl surface. Additionally, the alkaline pH conditions enhance the oxidation of MB by nZVAl. At pH 10, the MB removal efficiency increased significantly from 71.08 to 97.38% when the residence time was increased from 10 to 90 min, respectively. However, a further increase in residence time over 90 min showed a minor improvement in MB removal efficiency, reaching 98.44%. A reduction in MB removal was observed at pH 12, where the excess hydroxides in the solution competed with the negative ions on the nZVAl surface (Hamdy et al. 2019a, b). The same findings were reported in the literature. Hamdy et al. (2019a, b; Hamdy et al. 2018) have used another type of metal (nano zero-valent iron (nZVI)) and have reported an increase in MB removal with the increase in pH level. SADEK and MOSTAFA (2019) have reported that the MB dye is better removed in high alkaline media (pH ~ 10). Khosravi and Arabi (2016) have reported that a maximum MB removal efficiency of 76.5% was achieved at pH 9.5 using nZVI.

Effect of nZVAl dosage

The removal efficiencies of MB at different nZVAl dosages (0.1 g/L–1.0 g/L) are presented in Fig. 4b. For each nZVAl dosage, all experimental factors were kept constant at pH 10, an initial MB concentration of 10 mg/L, a stirring rate of 150 rpm, and a temperature of 30 °C, except residence time, which varied from 10 to 120 min. At a nZVAl dosage of 0.1 g/L, an increase in residence time from 10 to 120 min resulted in an improvement in MB removal efficiency from 42.17 to 58.09%, respectively. Additionally, the equilibrium time of MB dye adsorption was 90 min. At a residence time of 90 min, the MB removal efficiency improved from 58.09

to 97.38% when the nZVAl dosage was increased from 0.1 g/L to 1.0 g/L. This indicated a positive correlation between the nZVAl dosage and the MB removal efficiency. A direct correlation exists between the absorbent dosage and the number of free active sites, which leads to the adsorption of large amounts of dyes (Arabi and Sohrabi 2014; Hamdy et al. 2018; Kavitha and Namasivayam 2007). In a similar study, Hamdy et al. (2019a, b) used nZVI for MB adsorption, and they reported MB removal efficiencies of 91% at nZVI dosages of 2 g/L, using 10 mg/L initial dye concentration at residence time 30 min, pH 6, stirring rate 150 rpm, and temperature 30 °C. In another study, Salimi et al. (2019) investigated the adsorption of MB dye onto nano copper goethite (Cu-goethite), and they achieved removal efficiencies of 77 and 93% at Cu-goethite dosages of 0.001 and 0.2 g, respectively, using 10 mL of MB dye solution at a concentration of 40 mg/L at pH 9.

Effect of the initial MB concentration

The removal efficiencies of MB at different MB concentrations (10 mg/L–80 mg/L) are presented in Fig. 4c. For each MB concentration, all experimental factors were kept constant at pH 10, nZVAl dosage 1.0 g/L, stirring rate of 200 rpm, and temperature of 30 °C, except residence time which varied from 10 to 120 min. At an initial MB concentration of 10 mg/L, the removal efficiency increased from 78 to 100% when the residence time increased from 10 to 120 min, respectively. At 90 min of residence time, the removal efficiency of 99% was achieved at an initial MB concentration of 10 mg/L, which decreased to 80% with increasing the initial MB concentration to 80 mg/L. At high dye concentrations, an increase in intermolecular competition occurs on the sorbent surface due to the limited adsorption sites (Petala et al. 2013; Sadegh et al. 2017; Wei et al. 2019a). However, at low MB concentration, the percentage of the total adsorbate compounds to the surface active sites is low, and thus, the majority of the molecules can bond to the nanomaterial surface (Hamdy et al. 2019a, b; Mahmoud et al. 2021a, b, c, d; Pathania et al. 2017).

Effect of stirring rate

The removal efficiencies of MB at different stirring rates (100 rpm–300 rpm) are presented in Fig. 4b. For each stirring rate, all experimental factors were kept constant at pH 10, nZVAl dosage 1.0 g/L, an initial MB concentration of 10 mg/L, and temperature of 30 °C, except residence time which varied from 10 to 120 min. At a stirring rate of 100 rpm, the MB removal efficiency increased from 65.99% to 87.96% when the residence time was increased from 10 to 120 min. These results indicated that the MB removal efficiency continued to increase till the end of the

experiment, which may be due to insufficient residence time to reach a state of equilibrium (A. Hamdy et al. 2019a, b). At a stirring rate of 200 rpm, the MB removal efficiency increased with time, reaching the equilibrium condition after 90 min of residence time. A stirring rate of 200 rpm enhanced the solid–liquid phase mass transfer by increasing the chance of dye molecules coming into contact with nZVAl nanoparticles. Then, the MB removal efficiencies decreased by increasing the stirring rates to 250 rpm and 300 rpm, which is mainly due to the unstable attachment mechanism (El-Sayed 2011). At high stirring rates, a disturbance may occur to the electrostatic forces within the system (Djenouhat et al. 2008; Mahmoud et al. 2018a).

Effect of temperature

The removal efficiencies of MB at different adsorption temperatures (30 °C–60 °C) are presented in Fig. 4e. For each adsorption temperature, all experimental factors were kept constant at pH 10, nZVAl dosage of 1.0 g/L, an initial MB concentration of 30 mg/L, and a stirring rate of 200 rpm, except residence time, which varied from 10 to 120 min. At a temperature of 30 °C, the MB removal efficiency increased from 75 to 87%, when the residence time increased from 10 to 120 min. At 90 min of residence time, the removal efficiency of 85% was achieved at an adsorption temperature of 30 °C, which increased to 96% by increasing the adsorption temperature to 60 °C. At high temperatures, the activation energy barrier decreases, which results in an increasing rate of adsorption (Alharby et al. 2021a). Additionally, high adsorption temperatures may result in increasing the rate of intraparticle diffusion of MB molecules into the nZVAl (Doğan et al. 2004). Results also demonstrated that the equilibrium time decreased from 40 to 20 min, when the temperature increased from 30 to 60 °C, respectively. This indicates that the adsorption process of dye molecules onto nZVAl is most probably endothermic (Alguacil and López 2021).

Effect of detergents

Real dye wastewater may contain different types of detergents that are normally applied in the cleaning process. In this study, the effect of two liquid detergents (Vanish granules and Ariel) on MB removal efficiency was examined under the optimum operating conditions. As shown in Fig. 4f, the MB removal efficiency has decreased from 80% (no detergents added) to 75 and 54% after adding liquid Vanish granules at a concentration of 0.1 and 0.5 g/L, respectively, at 30 min residence time. Similar behaviors were observed for solutions containing liquid Ariel. This may be due to the competition between detergent substances and MB molecules for reactive/available sites, as well as the blocking that may occur to the adsorptive sites of the aluminum

nanoparticles, where a passive layer of detergent substances is formed and covers the nZVAl surface (Velusamy et al. 2021). Hamdy et al. (2018) stated that the existence of the phosphate groups in the detergents may play a key role in the formation of secondary minerals, which decrease the MB dye adsorption using nZVAl. However, a different behavior was observed when significantly increasing the concentration of the detergents in the solution from 0.5 to 5 g/L. An improvement in the MB removal efficiency was observed for a concentration of 5 g/L compared to 0.5 g/L for both types of detergents applied in this study. This result could be attributed to the generation of reactive oxygen species (ROS), which enhances the degradation of dye compounds (Arslan-Alaton et al. 2017; Asghar et al. 2015). Fenton's process uses O_2 with metal ions such as iron and/or aluminum to generate ROS (Asghar et al. 2015).

Effect of ionic strength

Real dye wastewater normally contains different types of inorganic salts, which are applied in large quantities during manufacturing, such as sodium chloride (NaCl), sodium sulfate (Na_2SO_4), and sodium carbonate (Na_2CO_3). The MB removal efficiency was examined by taking into consideration the ionic strength at pH 10, nZVAl dosage of 1.0 g/L, an initial MB concentration of 30 mg/L, a temperature of 30 °C, and stirring rate of 200 rpm, during residence time varied from 10 to 120 min. For example, at 30 min of residence time, the MB removal efficiency increased from 80.4 to 100% with increasing the Na_2SO_4 concentration in the solution from 0 to 8.43 M, respectively (Fig. 5a). Similar behavior was observed for NaCl and Na_2CO_3 (Fig. 5b, c). The salt ions play a key role in forcing MB molecules to aggregate and migrate toward the surface of the adsorbent, which significantly enhances removal efficiency. The enhancement in MB removal after adding salts could also be due to the dimerization of dye molecules in aqueous solutions (Kuo et al. 2008). Hamdy et al. (2018) found that an increase in Na_2SO_4 from 0 to 5 g/L caused an improvement in MB removal efficiencies from 96.8% to 99.5%, respectively, using an nZVI dosage of 10 g/L at 30 min residence time. Their study (Hamdy et al. 2018) also suggested that the dimerization of dye molecules and/or the dye molecules accumulation is the main reason for such improvement in dye removal. Satapanajaru et al. (2011) observed an improvement in the removal efficiencies of reactive red 198 (RR198) and reactive black 5 (RB5) dyes after increasing the NaCl concentration from 0.1 to 1% (w/v), using an nZVI dosage of 0.5 g/L. Satapanajaru et al. (2011) have reported that the pitting corrosion by NaCl played a great role in enhancing the degradation rates of dye compounds in the nano-treatment system. Bellir et al. (2012) observed an improvement in the removal efficiency of basic dye (Gentian
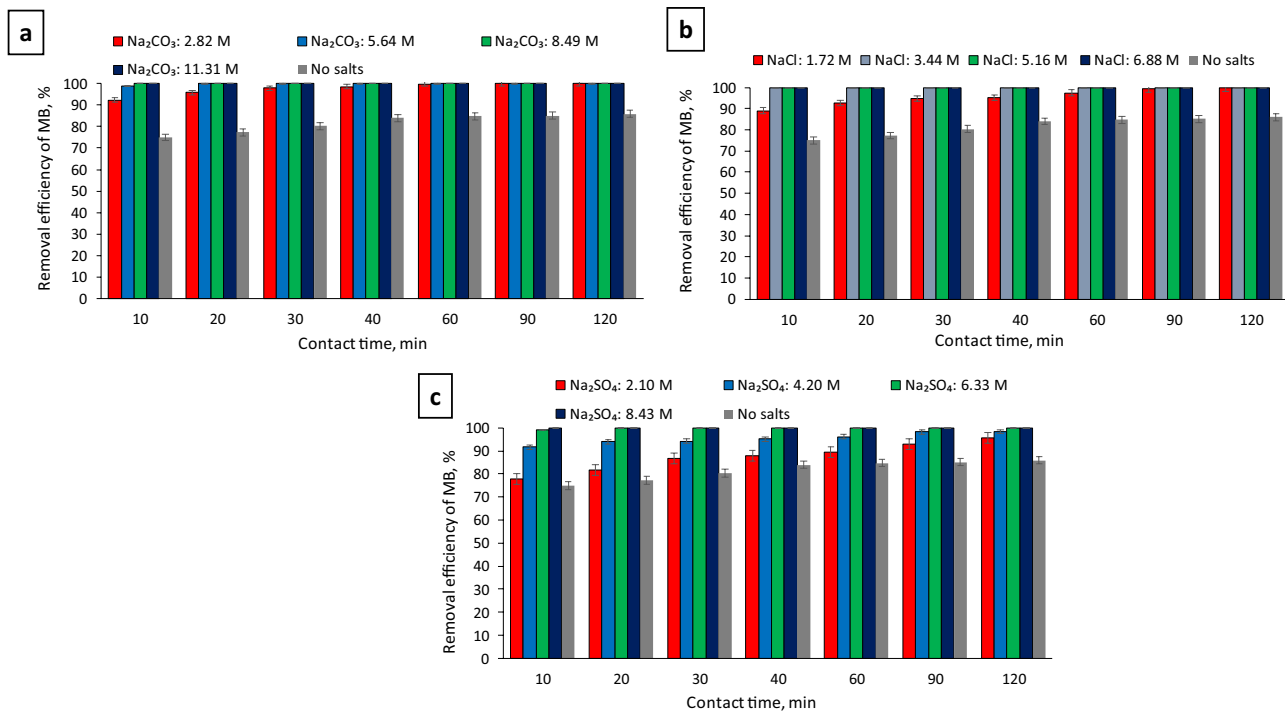
Fig. 5 Effects of adding salts on the removal efficiency of MB by nZVAl at $C_o = 30$ mg/L, pH 10, stirring rate 200 rpm, nZVAl dosage 1.0 g/L, and temperature 30 °C

Viole) by 9% after increasing the NaCl concentration from 0 to 0.1 M, using a bentonite dosage of 1.0 g/L at a 30 min residence time. Their study (Bellir et al. 2012) suggested that an increase in salt ions causes pressure on the thickness of the diffuse double layer, thus increasing the attractive force between adsorbate species and adsorbent particles. Bellir et al. (2012) also stated that an increase in salt ions could enhance the dye adsorption on the surface of adsorbents by forcing the dye molecules to aggregate. Yang et al. (2011) mentioned that the ionic strength also controls the absorption process, where the increase in ionic strength causes the absorption capacity to increase. The presence of Na^+ increases the absorption capacity of MB by reducing the interaction of MB molecules with H_2O, making it more amiable to graphene oxide (GO). Additionally, sodium ions inhibit the ionization of GO. It appears that the hydrophobicity of both MB and GO is enhanced by an increase in ionic strength. The control experiment (without the presence of GO) indicates that the removal of MB by direct centrifugation is not significantly affected by the increase in ionic strength when MB concentrations are low, where the adsorption capacity remained nearly unchanged. In addition, Zhang et al. (2021) reported the same behavior for the adsorption of MB by magnetic MOF with aluminum core/shell nanocomposite (Fe_3O_4@MIL-53(Al)), where they stated that the effect of ionic strength on adsorption is mainly reflected in two aspects: the salting-out effect and the competition

effect. Thus, in the case of the Fe_3O_4@MIL-53(Al) adsorption system for MB, the salting-out effect was dominant due to the increase in adsorption capacity on increasing the ionic strength. Accordingly, we suggest that the interaction of MB with nZVAl in the presence of salts follows a similar manner. However, a different behavior was observed by Fan et al. (2009). They stated that competition may occur between salt ions and dye molecules for the adsorptive sites in case the salt ions increase over a threshold level, which could hinder the removal of the dye.

Comparison of MB removal by various Adsorbents

Table 1 includes the removal efficiencies of MB dye by some adsorbent materials reported in the literature compared to nZVAl applied in this study. It was observed that there was a large variation in the removal efficiencies between different adsorbent materials, which is due to the variation in the experimental conditions (e.g., adsorbent dosage, pH, initial dye concentration). However, it is worth mentioning that nZVAl exhibited a higher MB removal efficiency than some adsorbents, such as biochar prepared from Eucalyptus sheathiana bark, spinel magnesium aluminate nanoparticles, *N. zanardinii macroalga*, date palm leaves, formaldehyde-treated sawdust, agricultural residue walnut shell, multi-walled carbon nanotubes, and zeolite synthesized from coal fly ash. The following adsorbent materials: nZVI, sulfuric

Table 1 Removal efficiencies of MB dye from aqueous solutions using various adsorbents

Adsorbent	Experimental factor						Removal efficiency	Langmuir Isotherm Q_m (mg/g)	Freundlich isotherm K_F (mg/g)·(L/mg)$^{1/n}$	Pseudo-first-order q_e (mg/g)	Pseudo-second-order q_e (mg/g)	References
	Adsorbent dosage (g/L)	pH	Initial MB conc. (mg/L)	Residence time	Temp. (°C)	Stirring rate						
nZVAl	1.0	10	10–80	120 min	30	200 rpm	78–100%	4.24	1.45	3.22	26.2	This study
nZVI	10	6	10–70	30 min	30	150 rpm	95.6–100%	5.53	1.59	1.052	4.836	(Hamdy et al. 2019a, b)
Bio-char prepared from Eucalyptus sheathiana bark	0.02	11.3	10–100	150 min	35	130 rpm	38–75%	104.17	0.02	–	40.3	(Dawood et al. 2016)
Formaldehyde treated sawdust	4	7	50	30–45 min	26±1	160 rpm	92.1–92.8%	–	–	–	–	(Garg et al. 2004)
Kaolin	0.5	10	100	120 min	25	–	100%	72.57	–	–	36.98	(Mouni et al. 2018)
Sulfuric acid-treated sawdust	4	7	50	30–45 min	26±1	160 rpm	99.4–99.5%	–	–	–	–	(Garg et al. 2004)
Oil palm wastes-derived activated carbons	5	2	50	90 min	–	150 rpm	95.71–98.09%	44.8	14.38	25.91	45.25	(Baloo et al. 2021)
Activated carbon	4	7	50	30–45 min	26±1	160 rpm	100%	–	–	–	–	(Garg et al. 2004)
Activated carbon	0.5	2–9	40–120	5 h	25	WBO*	98.0–99.6%	270.27	236.23	933.3	263.2	(Li et al. 2013a, b)
Jute fiber carbon	0.4–4	6	50	4 h	28	120 rpm	40.1–100%	225.64	–	–	–	Senthilkumaar et al. (2005)
Agricultural residue Walnut Shell	1.25	6	20	2 h	25	–	97.1%	51.55	18.8	2.494	28.99	(Tang et al. 2017)
Coir pith carbon	2–12	6.9	10	30 min	35	200 rpm	97.3–100%	5.87	1.192	0.6108	–	(Kavitha and Namasivayam, 2007)
Titanium dioxide nanoparticles	1.2	7	15	30–60 min	–	–	97.7–100%	–	–	–	–	(Rahimi et al. 2016)

Table 1 (continued)

Adsorbent	Experimental factor							Removal efficiency	Langmuir Isotherm Q_m (mg/g)	Freundlich isotherm K_F (mg/g)·(L/mg)$^{1/n}$	Pseudo-first-order q_e (mg/g)	Pseudo-second-order q_e (mg/g)	References
	Adsorbent dosage (g/L)	pH	Initial MB conc. (mg/L)	Residence time	Temp. (°C)	Stirring rate							
Tea waste	10	11	100	24 h	35	150 rpm	98%	113.1	21.3	23.32	24.077	(Liu et al. 2018)
Graphene oxide	0.5	2–9	40–120	5 h	25	WBO*	94.8–98.8%	243.90	114.86	1995.6	243.9	(Li et al. 2013a, b)
Activated carbon prepared from Pea Shells (Pisum sativum)	1.0	6.85	100–350	120 min	25	150 rpm	65–100%	246.9	119.32	84.86	201.21	(Geçgel et al. 2013)
Multi-walled carbon nanotubes	0.5	2–9	40–120	5 h	25	WBO*	72.4–82.7%	188.68	54.03	199.5	196.1	(Li et al. 2013a, b)
Zeolite synthesized from coal fly ash	7.5	10.4–11.0	350	4 h	20±0.1	200 rpm	60–98%	23.70	–	–	–	(Sun et al. 2010)
Spinel magnesium aluminate nanoparticles	0.1	7.0	3	160 min	25	–	84%	0.945	0.646	–	–	(Ismail et al. 2013)
Wheat shells	3.0	2–4	100–400	75 min	30	150 rpm	70–95%	16.56–21.50	0.53–1.46	13.7–21.66	17.92–32.26	(Bulut and Aydin, 2006)
N. zanardinii macroalga	6	6.5	160	120 min	27	150 rpm	80%	95.45	1.13	16.09	17.86	(Daneshvar et al. 2017)
Date palm leaves	10	6.5	200	160 min	30	100 rpm	66.1%	43.10–58.14	0.54–2.03	15.136	15.152	(Gouamid et al. 2013)
Activated lignin-chitosan pellets	2.0	2–9	43.65	40 h	20	110 rpm	49–80%	36.25	7.02	4.266–26.44	4.448–29.04	(Albadarin et al. 2017)
Sewage Sludge Ash Pellets	30.0	10	25.0	60 min	25	250 rpm	98%	2.56	0.824	–	–	(El-Deen et al. 2022)

*WBO: water bath oscillator

acid-treated sawdust, oil palm waste-derived ACs, coir pith carbon, titanium dioxide nanoparticles, wheat shells, and tea waste exhibited a comparable MB removal efficiency to nZVAl but using higher dosages of these adsorbents. In addition, AC, graphene oxide, jute fiber carbon, and kaolin exhibited a comparable MB removal efficiency to nZVAl, but at a lower dosage. However, the nZVAl achieved 100% removal efficiency at a slower reaction time compared to these four adsorbents.

Adsorption isotherm

Isotherm studies are employed using Langmuir and Freundlich isotherms to explain the adsorption equilibrium between MB molecules and the nZVAl.

Langmuir isotherm model

The Langmuir isotherm describes the adsorption process based on some assumptions (Langmuir 1918): (1) adsorption of molecules occurs in only one layer on the surface of the adsorbent (monolayer adsorption); (2) adsorption takes place at specific homogeneous sites; and (3) strong attraction occurs between the surface of the adsorbent and the adsorbate (Langmuir and Waugh 2002). The linearized form of the Langmuir isotherm model is presented in Eq. (9) (Mahmoud and Mahmoud 2022).

$$\frac{C_e}{q_e} = \left(\frac{1}{Q_m}\right)C_e + \frac{1}{K_L \cdot Q_m} \qquad (9)$$

where C_e is the MB dye concentration in the aqueous solution at equilibrium (mg/L), Q_m is the maximum adsorption capacity, q_e is the amount of MB molecules adsorbed at equilibrium per gram of nZVAl (mg/g), and K_L is the Langmuir constant (L/mg).

Figure 6a shows a linear plot of C_e/q_e (g/L) versus C_e (mg/L), which gives an intercept of $1/(K_L \times Q_m)$ and a slope of $1/Q_m$. The model constants are $Q_m = 4.24$ mg/g and $K_L = 0.122$ L/mg. The coefficient of determination (R^2) for the Langmuir model was calculated as 0.8253. The low R^2 value indicates a poor model fit when compared with the experimental data. Therefore, the removal of MB dye by nZVAl did not follow the monolayer adsorption process.

Freundlich isotherm model

Freundlich's isotherm assumption is based on the formation of a heterogeneous surface of the adsorbates on the adsorbent surface (Ahmed Hamdy et al. 2019a, b). Equation (10) represents the linearized form of the Freundlich isotherm model (Hamdy et al. 2021).

$$\log(q_e) = \left(\frac{1}{n}\right)\log(C_e) + \log(K_F) \qquad (10)$$

where K_F is the Freundlich constant describing the multilayer adsorption capacity $(mg/g)\cdot(L/mg)^{1/n}$, and $1/n$ is the Freundlich constant describing the adsorption intensity/strength.

Figure 6b shows a linear plot of $\log(q_e)$ (mg/g) versus $\log(C_e)$ (mg/L), which gives an intercept of $\log(K_F)$ and a slope of $1/n$. A high R^2 value (0.9569) indicated a good model fit when compared with the experimental data and suggests that multilayer adsorption played a great role in MB dye removal. The results also indicated that the heterogeneous adsorbent surface of nZVAl resulted in a high affinity toward cationic dye (MB). The model constants are $1/n = 0.4926$ L/g and $K_F = 1.45$ $(mg/g)\cdot(L/mg)^{1/n}$. The value of $1/n$ is less than unity, demonstrating the favorable adsorption of MB molecules onto nZVAl. Table 1 includes the isotherm model constants for the adsorption of MB by some adsorbent materials reported in the literature compared to the nZVAl applied in this study. The nZVAl achieved higher adsorption capacity than coir pith carbon (Kavitha and Namasivayam 2007), biochar prepared from eucalyptus sheathiana bark (Dawood et al. 2016), spinel magnesium aluminate nanoparticles (Ismail et al. 2013), *N. zanardinii macroalga* (Daneshvar et al. 2017), date palm leaves (Gouamid et al. 2013), and wheat shells (Bulut and Aydin 2006), but lower than oil palm waste-derived ACs (Baloo et al. 2021), AC (Li et al. 2013a, b), agricultural residue walnut shell (Tang et al. 2017), tea waste, graphene oxide (Li et al. 2013a, b), AC prepared from pea shells (Geçgel et al. 2013), activated lignin-chitosan pellets (Albadarin et al. 2017), and multi-walled carbon nanotubes (Li et al. 2013a, b;).

Kinetic studies

Kinetic studies are employed using pseudo-first-order (PFO), pseudo-second-order (PSO), and intraparticle diffusion models to quantitatively understand the kinetic adsorption of MB onto nZVAl.

Pseudo-first-order

The PFO model assumes that physical adsorption (physisorption) occurs between adsorbate species and adsorbent particles, and both hydrogen bonds and van der Waals forces have a great impact on the bonding between sorbate and sorbent (Mahmoud et al. 2019; Wu et al. 2021). Equation (11) represents the linearized form of the pseudo-first-order model (Abdelmigeed et al. 2022).
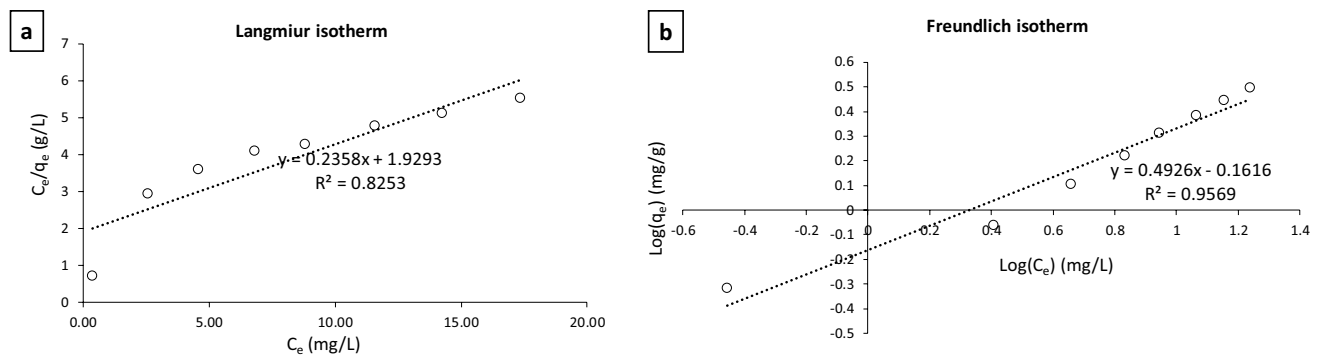
Fig. 6 Isotherm studies for the adsorption of MB dye onto nZVAl: **a** Langmuir model (linear form), **b** Freundlich model (Linear form)

$$\log \left(q_e - q_t \right) = \log \left(q_e \right) - \frac{k_1}{2.303} t \tag{11}$$

where k_1 is the pseudo-first-order constant (mg/g min) and q_t and q_e are the amounts of adsorbed molecules at time t and equilibrium, respectively (mg/g).

Figure 7a shows a linear plot of time versus $\log(q_e–q_t)$, which gives an intercept of $\log(q_e)$ and a slope of $-k_1/2.303$. The model constants are $q_e = 3.22$ mg/g and $k_1 = 0.0274$ min^{-1}. The coefficient of determination (R^2) for the pseudo-first-order model was calculated as 0.9016. Although the R^2 value for the pseudo-first-order model is high, it is lower than the R^2 value for the pseudo-second-order model, which will be discussed in the following section. Therefore, the pseudo-first-order equation is not the best model to describe the kinetic adsorption of MB onto nZVAl.

Pseudo-second-order

The pseudo-second-order (PSO) model assumes that a chemisorption reaction commonly occurs, in which electrons are covalently exchanged or shared between sorbate and sorbent (Ho and McKay 1999; Mahmoud et al. 2022). Equation (12) represents the linearized form of the pseudo-second-order model.

$$\frac{t}{q_t} = \frac{1}{k_2 x q_e^2} + \frac{1}{q_e} t \tag{12}$$

where k_2 is pseudo-second-order constant (g/mg.min).

Figure 7b shows a linear plot of time versus t/q_t, which gives an intercept of $1/(k_2 \times q_e^2)$ and a slope of $1/q_e$. The model constants are $q_e = 26.2$ mg/g and $k_2 = 0.0212$ (g/mg.min). A high R^2 value (0.9999) indicated a good model fit when compared with the experimental data and suggests that chemisorption plays a great role in MB dye removal, where a chemical bond occurs between MB molecules and the active sites of the nanoparticles. Additionally,

the adsorption capacity obtained from the experiment ($q_{e,\text{ exp}} = 26.0$ mg/g) was close to the one calculated by the model ($q_{e,\text{ cal}} = 26.2$ mg/g). Table 1 includes the kinetic model constants for the adsorption of MB by some adsorbent materials reported in the literature compared to the nZVAl applied in this study. The nZVAl achieved a higher adsorption capacity than activated lignin-chitosan pellets, date palm leaves, wheat shells, *N. zanardinii macroalga*, tea waste, and nZVI.

Intraparticle diffusion model

Equation (13) represents the intraparticle diffusion equation, which is mainly applied to describe the different adsorption stages (surface and pore volume diffusions) (WeberJr. and Morris, 1963).

$$q_t = k_p \cdot t^{0.5} + C \tag{13}$$

where C is the model constant (mg/g), and k_p is the intraparticle diffusion model rate constant (mg/g/min$^{0.5}$).

Figure 7c shows a plot of $t^{0.5}$ versus q_t, generating two straight lines with different slopes. In the initial phase, a faster mass transfer of ions to the adsorbent boundary layer occurred externally ($k_p = 0.914$ mg/g/min$^{0.5}$). In the following stage, the intraparticle diffusion of ions is considerably slow inside the adsorbent pores ($k_p = 0.1568$ mg/g/min$^{0.5}$).

Thermodynamic study

Van't Hoff and Gibbs–Helmholtz equations were used to compute the thermodynamic characteristics of MB adsorption on nZVAl under various temperatures (303, 313, 323, and 333 K). These parameters include Gibbs free energy ($G°$), enthalpy ($H°$), and entropy ($S°$) (Eqs. (14–17)):

$$\Delta G° = \Delta H° - T \Delta S° \tag{14}$$
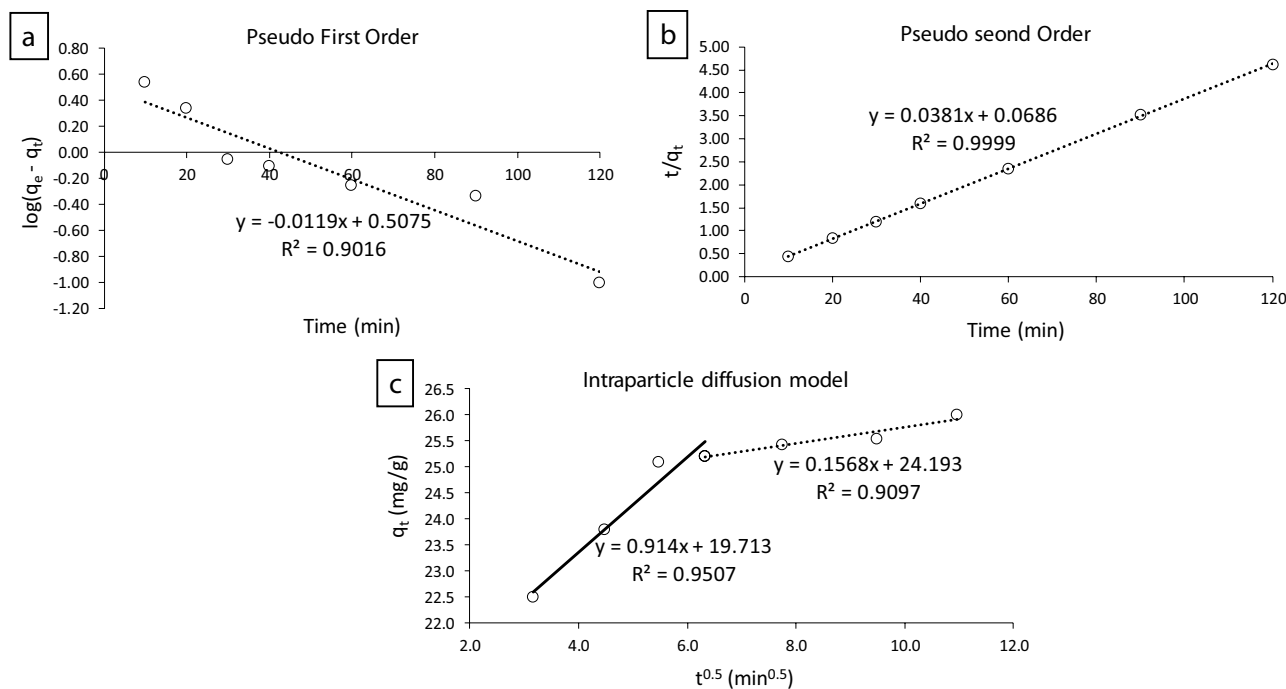
$$\Delta G° = -RT \ln K° \tag{15}$$

Fig. 7 Kinetic studies for the adsorption of MB dye onto nZVAl: **a** Pseudo-first-order model (linear form), **b** Pseudo-second-order model (linear form), **c** Intraparticle diffusion model (linear form)

$$\ln K^{\circ} = \frac{-\Delta H^{\circ}}{RT} + \frac{\Delta S^{\circ}}{R} \qquad (16)$$

$$K^{\circ} = \frac{q_e}{C_e} \qquad (17)$$

where K° is the equilibrium constant (mL/g), C_e is the equilibrium concentration of MB (mg/L), q_e is the uptake amount of MB at equilibrium (mg/g), T is the absolute temperature (K), R is the gas constant (J mol^{-1} K^{-1}), and ΔH° (J/mol) and ΔS° (J deg^{-1} mol^{-1}) were determined from the slope and intercept of plot $\ln K^{\circ}$ versus $1/T$, respectively (Hamdy 2021).

Batch experiments of MB removal were performed at different operating temperatures ranging from 303 to 333 K in order to evaluate the effect of temperature on the removal of MB by nZVAl nanoparticles where the uptake of MB dye increased with increasing temperature at the same adsorption time. Van't Hoff and Gibbs–Helmholtz equations were used to compute the thermodynamic parameters such as Gibbs free energy (ΔG°), enthalpy change (ΔH°), and entropy change (ΔS°). The calculated ΔG° values for the adsorption of MB dye onto nZVAl nanoparticles at all temperatures are shown in Fig. 8a and listed in Table 2. The values of ΔH° and ΔS° were determined from the slopes and intercepts of the plot of $\ln K^{\circ}$ vs $1/T$ (Fig. 8b) and are also listed in Table 2. It could be observed that with an increase in the temperature from 303 to 333 K, the K° values

raised from 307.14 to 739.47 mL/g, respectively. This suggests that the high temperatures increase the interactions between the MB molecules and the nZVAl nanoparticles. The positive value of ΔH° (+23.217 kJ/mol) demonstrates the endothermic nature of the removal process and reveals that the adsorption process is an energy-consumption process because, at relatively high temperatures, the dye effluents are usually produced and increase the diffusion of the dye in the solution, which increases the dye adsorption rate. This supports the results obtained earlier where the MB dye uptakes increase with the increase in solution temperature (Soldatkina and Yanar 2021).

While the enthalpy range for physisorption is between 20 and 40 kJ/mol, the value for chemisorption is between 80 and 400 kJ/mol (Chowdhury et al. 2012). Thus, the positive value and low heat quantity required for enthalpy demonstrated that MB adsorption was physically natural. Although the process was physical in nature, as the temperature increased, the nZVAl nanoparticles' capacity also increased. This result was explained by the fact that the vibrational energies of MB molecules increased as they reacted with nZVAl nanoparticles at high temperatures. In terms of enthalpy value, the ion exchange reaction is typically between physical adsorption and chemical sorption. However, in our study, based on thermodynamic investigation, the process was identified as physical adsorption because the ΔH° value is 23.217 kJ/mol. The isotherm form of MB adsorption onto nZVAl nanoparticles suggests

that solid–solid attractive forces were prominent in MB adsorption, indicating the occurrence of physical monolayer adsorption. Similar results were also observed in the literature (Fil et al. 2014).

Additionally, the positive values of $\Delta S°$ represented that the degree of freedom and randomness at the solid–liquid interface irregularly increased with concentration decreased during the adsorption process. These results were achieved due to the strong solute–solute attractive interactions, which boosted the adsorption of MB onto nZVAl nanoparticles' surface and reduced the rate of adsorption–desorption (Wei et al. 2019b). On the contrary, the negative $\Delta G°$ values (−14.427 to −18.288 kJ/mol) suggested that the feasibility of MB removal by nZVAl nanoparticles and the adsorption process was of spontaneous nature. In addition, the decrease in the value of $\Delta G°$ with an increase in the temperature of the solution has demonstrated that the adsorption of MB is thermodynamically favored at higher temperatures, and the adsorption mechanism is physisorption. This phenomenon has also been observed in the adsorption of MB onto peat (Fernandes et al. 2010) and onto AC at different ionic strengths (Ghasemi and Asadpour 2007).

Activation parameters

From the pseudo-second-order rate constant k_2 (Table 3), the activation energy E_a for adsorption of MB onto nZVAl

nanoparticles was determined using the Arrhenius equation (Eq. (18)) (Alharby et al. 2021b):

$$\ln k_2 = \ln A - \frac{\Delta E_a}{RT} \tag{18}$$

where A is the Arrhenius constant, k is the rate constant, R is the gas constant (8.314 J mol^{-1} K^{-1}), ΔE_a is the activation energy (kJ mol^{-1}), and T is the temperature (K). ΔE_a can be obtained from the slope of a plot of ln k_2 vs 1/T.

The degree of activation energy may provide insight into the type of sorption. Adsorption can be classified as either a physical or chemical type. Because the forces involved in physical adsorption are weak, the activation energy is usually < 40 kJ mol^{-1}. While the chemical reaction process is represented by higher values because chemical adsorption is more specific and involves forces that are much stronger than in physical adsorption. In this work, the slope and intercept of the ln k_2 vs 1/T plot were used to determine the values of ΔE_a and A (Fig. 9). The ΔE_a was calculated to be 17.65 kJ mol^{-1} and A to be 18.65 g.mg^{-1}.min^{-1} for the adsorption of MB on nZVAl nanoparticles (Table 3). It was easily concluded that the activation energy value was positive and lower than 40 kJ/mol indicating that the feasibility of the adsorption process and that the process might involve active physical adsorption. Consequently, the adsorption process is physically diffusion-controlled, and intra-particle diffusion is the rate-limiting step in adsorption. Accordingly,
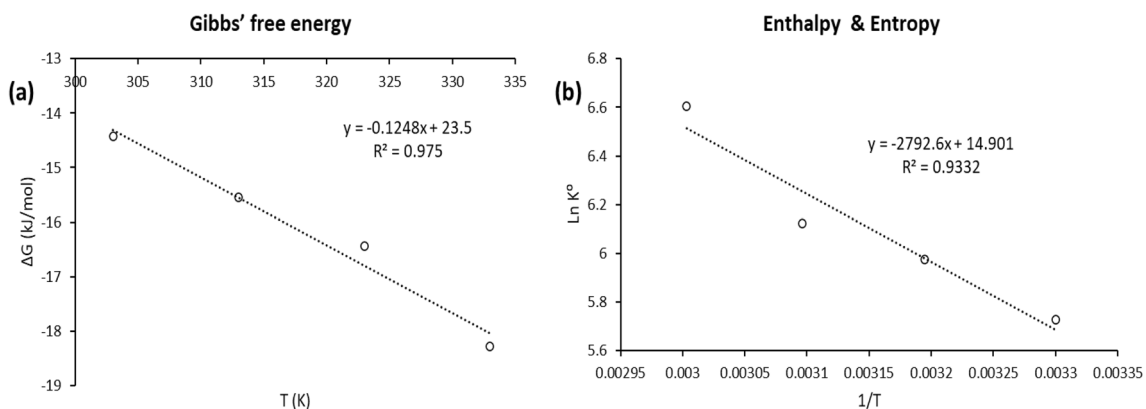

Fig. 8 **a** Plot of Gibbs' free energy change vs temperature, **b** Plot of ln $K°$ vs 1/T to determine the enthalpy ($\Delta H°$) and entropy ($\Delta S°$)

Table 2 The thermodynamic parameters and the distribution and adsorption constants for the adsorption of MB onto nZVAl nanoparticles ([MB] = 30 mg/L; nZVAl dosage = 1 g/L) at different temperatures

T (°K)	$K°$ (mL/g)	Ln $K°$	$\Delta G°$ (kJ/mol)	$\Delta H°$ (kJ/mol)	$\Delta S°$ (J deg^{-1} mol^{-1})	R^2
303	307.14	5.7273	−14.427	23.217	124.24	0.9332
313	393.78	5.9758	−15.550		49.682	
323	456.58	6.1237	−16.444		50.913	
333	739.47	6.6059	−18.288		54.921	

the MB adsorption onto nZVAl is expected to occur by spontaneous and endothermic physisorption. This agrees with other results of this study, and with the results of Suteu and Malutan (2013).

Artificial neural network

Adjusted weights and biases

A weight matrix ($W_{10 \times 11}$) was generated as a result of the connection between each hidden layer neuron and each component of the input vector ($P_{11 \times 1}$). A net input ($u10 \times 1 = \Sigma W_{10 \times 11} \cdot P_{11 \times 1} + b_{10 \times 1}$) was produced after adding the weighted input ($\Sigma W_{10 \times 11} \cdot P_{11 \times 1}$) to the 10-length bias ($b_{10 \times 1}$). The "tansig" function is used to transfer this net input to the output layer. A weight matrix ($W_{1 \times 10}$) was generated because of the connection between the output layer single neuron and each hidden layer neuron ($P_{10 \times 1}$). A net input ($u_{1 \times 1} = \Sigma W_{1 \times 10} \cdot P_{10 \times 1} + b_{1 \times 1}$) was produced after adding the weighted input ($\Sigma W_{1 \times 10} \cdot P_{10 \times 1}$) to 10-length bias ($b_{1 \times 1}$). The "tansig" function is then used to transfer this net input to the output layer." function is used to transfer this net input to the output layer.

Training and validation performance

As shown in Fig. 10a, the training step was conducted with (6) validation checks and the gradient magnitude (2.3989) exceeded the least error level ($1e^{-5}$). Since the maximum allowable number of validation checks is 6 epochs, the training step was terminated for this reason. Figure 10b shows a plot of MSE versus epoch number. For the training step, a normal trend was observed and the MSE reduced gradually, where the lowest value was recorded at epoch 6. For both the validation and test steps, the MSE increased gradually after epoch 0. This trend for the validation step indicates data overfitting. The best validation performance was reported as 10.7804 at epoch 0.

Regression plot

Figure 10c shows a plot of network targets versus network outputs. The dashed and solid lines indicate the perfect result and the best-fitting, respectively. The R^2 values
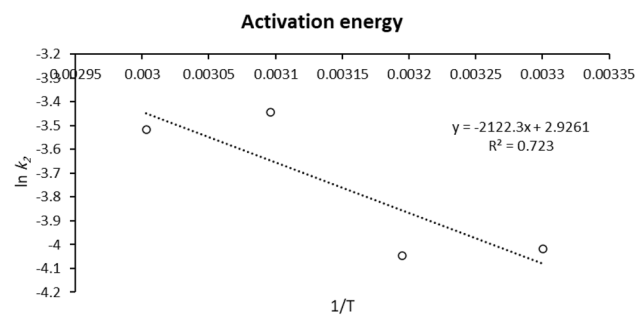

Fig. 9 The plot of rate constant (ln k_2) vs temperature (1/T) to determine the activation energy (ΔE_a) of the reaction

were reported as 0.974 for training, 0.970 for validation, and 0.960 for testing, which indicates a strong correlation between the output and the target data. The proposed model was also proved to be reliable in predicting the MB removal efficiency, where the overall R^2 value was 0.970. Consequently, 97% of the variations in MB removal efficiency by nZVAl were explained by the 11 parameters considered in this study (residence time, initial MB concentration, temperature, pH, stirring rate, nZVI dosage, the concentration of two detergents: Ariel and Vanish, and the concentration of three salts: NaCl, Na_2CO_3, and Na_2SO_4). Thus, the created ANN can be a useful tool in precisely estimating the MB removal efficiency, taking into consideration the studied range.

Cost estimation of scaling up the adsorption unit

In this section, the Capital Expenditures (CAPEX) and the Operating Expenses (OPEX) were calculated based on a study by (Hamdy et al. 2019a, b), which used iron nanoparticles to remove MB from aqueous solutions. The cost was estimated based on the optimal operating conditions obtained during lab experiments.

Amortization cost (AC)

The amortized cost represents the annual interest expenditures out of the capital costs over the lifetime of the treatment unit. The capital cost was multiplied by an amortization factor (α) for AC estimation (Eq. (19)).

Table 3 Activation parameters for adsorption of MB onto nZVAl nanoparticles ([MB] = 30 mg/L; nZVAl dosage = 1 g/L) at different temperatures

T	1/T	k_2 (g mg^{-1} min^{-1})	ln k_2	ΔE_a (kJ mol^{-1})	A (g mg^{-1} min^{-1})	R^2
303	0.0033	0.018	−4.0173	17.644	18.654	0.723
313	0.003195	0.0175	−4.04555			
323	0.003096	0.0319	−3.44515			
333	0.003003	0.0297	−3.51661			

$$AC \left(\$/m^3\right) = \left(\frac{I}{V.D} x \frac{t_R}{t_W} \right) x \alpha \tag{19}$$

where AC is the expenses per m^3 of treated wastewater, α is an amortization factor (Eq. (20)), I is the annual amortization cost obtained from local providers (i.e., 5000 \$/year), t_W is the daily working hours (i.e., 18 h/day), t_R is the treatment time (i.e., adsorption time = 90 min), D is the operating days per year (assuming 260 days/year), V is the volume of treatment tank (m^3), and D is the yearly operating days (assuming 260 days/year) (Eq. (21)).

$$\alpha = \frac{i(1 + i)^L}{(1 + i)^L - 1} \tag{20}$$

$$V = Q x \frac{t_R}{t_w} \tag{21}$$

where i is the annual interest rate (assuming 0.04%), Q is the daily wastewater discharge (m^3/day), and L is the lifetime (i.e., 10 years).

Operating cost (OC)

The OC was calculated by summing the following three items: (1) cost of reagent (material), (2) maintenance cost, and (3) energy cost (Gar Alalm and Nasr 2018). Equation (22) was used to estimate the cost of reagents (e.g., for pH adjustment). The cost of labor was excluded from this study since the same labor working in the facility will operate the treatment unit.

$$RC = C \times P \tag{22}$$

where RC is the reagent cost per m^3 of treated wastewater (\$/m^3), P is the cost per gram of reagent (\$/g), and C is chemical dosage (g/m^3).

Equation (23) was used for energy cost estimation.

$$EC = \frac{Ext_W}{Q} \tag{23}$$

where E is the hourly cost of electricity (\$/h), and EC is the energy cost per m^3 of treated wastewater (\$/m^3). The maintenance cost was assumed 2% of the yearly investment (MC = 0.02 × AC).
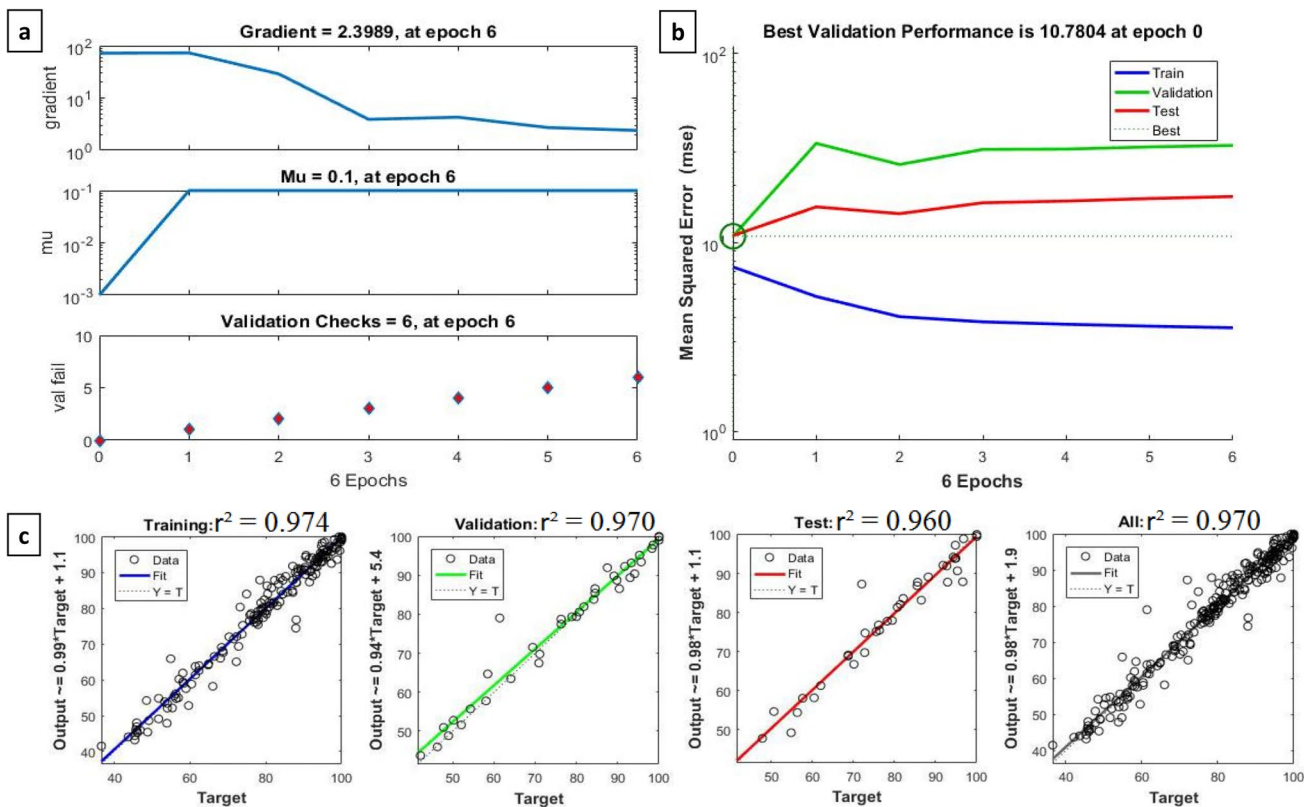
Fig. 10 Prediction of MB removal efficiency using ANN: **a** training performance, **b** best validation performance, and **c** regression plot between target and output

Table 4 Cost estimation of scaling up the adsorption unit for treating MB dye for an industry with a capacity of 100 m³/day

Item	Cost (US$/m³)	Percentage (%)
Amortized cost (AC)	0.16	12.2
Adsorbent material	1.0	76.1
Electricity	0.15	11.4
Maintenance	0.0032	0.2
Total cost	1.31	100

Total cost (TC)

The cost was estimated by assuming the daily flow rate is about 100 m³ (Table 4). In this case, the volume of the adsorption tank will be 8.33 m³. Consequently, the AC was estimated at US$ 0.16/m³, equivalent to 12.2% of the TC. The EC was calculated as US$0.15/m³ using an electricity tariff of US$ 0.10/kWh (A. S. Mahmoud et al. 2021c). The RC cost for adsorbent material was about US$ 1.0/m³. The MC was estimated at US$ 0.0032/m³. Therefore, the OC was 1.15 \$/m³ (i.e., 87.8% TC), resulting in a TC of US$ 1.31/m³. In a comparable study, (Mahmoud et al. 2021c) found that the total cost of treating real textile wastewater using an adsorption process (nano bimetallic iron/copper (Fe/Cu)) was US$ 6.0/m³. Hamdy et al. (2018) also found that the total cost of removing MB from aqueous solutions using the adsorption process (iron nanoparticles) was US$ 1.66/m³.

Conclusion

This study demonstrated that the nZVAl particles are effective in the adsorption of MB from aqueous solutions. A removal efficiency of 99% was achieved at an initial MB concentration of 10 mg/L, pH 10, nZVAl dosage of 1.0 g/L, stirring rate of 200 rpm, the temperature of 30 °C, and an equilibrium time of 90 min. A reduction in MB removal efficiency was observed in the presence of detergents, while the presence of inorganic salts resulted in an improvement in MB removal efficiency. The adsorption data were well described by the Freundlich isotherm model (R^2: 0.9569, $K_F = 1.45$ (mg/g)·(L/mg)$^{1/n}$) and the pseudo-second-order kinetic model (R^2: 0.9999, $q_e = 26.2$ mg/g). Based on the thermodynamic study, the positive value of $\Delta H°$ ($+23.217$ kJ/mol) demonstrated the endothermic nature of the removal process and reveals that the adsorption process is an energy-consumption process. The enthalpy positive value and low heat quantity required for enthalpy demonstrated that MB adsorption was physically natural. The total treatment cost, including capital expenditures and operating expenses, is about US$ 1.31 per cubic meter. Under the studied 11 parameters, the ANN model was able to precisely predict the MB removal efficiency with an R^2 value of 0.97. This model can also be used to maximize MB uptake by nZVAl under different environmental conditions.

Declarations

Conflict of interest The authors declare that they have no competing interests.

References

Abdelmigeed MO, Sadek AH, Ahmed TS (2022) Novel easily separable core–shell Fe₃O₄/PVP/ZIF-8 nanostructure adsorbent: optimization of phosphorus removal from fosfomycin pharmaceutical wastewater. RSC Adv 12:12823–12842. https://doi.org/10.1039/D2RA00936F

Albadarin AB, Collins MN, Naushad M, Shirazian S, Walker G, Mangwandi C (2017) Activated lignin-chitosan extruded blends for efficient adsorption of methylene blue. Chem Eng J 307:264–272. https://doi.org/10.1016/J.CEJ.2016.08.089

Alguacil FJ, López FA (2021) Organic dyes versus adsorption processing. Molecules. https://doi.org/10.3390/MOLECULES26185440

Alharby NF, Almutairi RS, Mohamed NA (2021a) Adsorption behavior of methylene blue dye by novel crosslinked o-cm-chitosan hydrogel in aqueous solution: kinetics, isotherm and thermodynamics. Polym 13(21):3659. https://doi.org/10.3390/POLYM13213659

Aljeboree AM, Alshirifi AN, Alkaim AF (2017) Kinetics and equilibrium study for the adsorption of textile dyes on coconut shell activated carbon. Arab J Chem 10:S3381–S3393. https://doi.org/10.1016/J.ARABJC.2014.01.020

Alqadami AA, Naushad M, Abdalla MA, Khan MR, Alothman ZA (2016) Adsorptive removal of toxic dye using Fe₃O₄−TSC nanocomposite: equilibrium, kinetic, and thermodynamic studies. J Chem Eng Data 61:3806–3813. https://doi.org/10.1021/ACS.

JCED.6B00446/ASSET/IMAGES/MEDIUM/JE-2016-00446V_0008.GIF

Alshehri AA, Malik MA (2019) Biogenic fabrication of ZnO nanoparticles using trigonella foenum-graecum (Fenugreek) for proficient photocatalytic degradation of methylene blue under UV irradiation. J Mater Sci Mater Electron 30:16156–16173. https://doi.org/10.1007/S10854-019-01985-8/FIGURES/12

Amor N, Noman MT, Petru M (2021) Prediction of methylene blue removal by nano Tio$_2$ using deep neural network. Polym 13(18):3104. https://doi.org/10.3390/POLYM13183104

Arabi S, Sohrabi MR (2014) Removal of methylene blue, a basic dye, from aqueous solutions using nano-zerovalent iron. Water Sci Technol 70:24–31. https://doi.org/10.2166/WST.2014.189

Arslan-Alaton I, Olmez-Hanci T, Arslan-Alaton I, Olmez-Hanci T (2017) The use of Al and Fe nanoparticles for the treatment of micropollutants. Nanotechnol Environ Remediat Appl Implic. https://doi.org/10.1007/978-3-319-53162-5_3

Asghar A, Raman AAA, Daud WMAW (2015) Advanced oxidation processes for in-situ production of hydrogen peroxide/hydroxyl radical for textile wastewater treatment: a review. J Clean Prod 87:826–838. https://doi.org/10.1016/J.JCLEPRO.2014.09.010

Baloo L, Isa MH, Sapari NB, Jagaba AH, Wei LJ, Yavari S, Razali R, Vasu R (2021) Adsorptive removal of methylene blue and acid orange 10 dyes from aqueous solutions using oil palm wastes-derived activated carbons. Alex Eng J 60:5611–5629. https://doi.org/10.1016/J.AEJ.2021.04.044

Bao Y, Zhang G (2012) Study of adsorption characteristics of methylene blue onto activated carbon made by salix psammophila. Energy Proced 16:1141–1146. https://doi.org/10.1016/J.EGYPRO.2012.01.182

Bellir K, Sadok Bouziane I, Boutamine Z, Bencheikh Lehocine M, Meniai AH (2012) Sorption study of a basic dye gentian violet from aqueous solutions using activated bentonite. Energy Proced 18:924–933. https://doi.org/10.1016/J.EGYPRO.2012.05.107

Bulut Y, Aydin H (2006) A kinetics and thermodynamics study of methylene blue adsorption on wheat shells. Desalination 194:259–267. https://doi.org/10.1016/J.DESAL.2005.10.032

Chao YX, Jun W, Peifang H, Guoxiang W, Lingzhan Y, Bowen M, Yangyang L, Zhang YF, Xu Y, Wang C, Hou J, Wang P, You G, Miao L, Lv B, Yang Y, Zhang F (2017) Application of zero valent iron coupling with biological process for wastewater treatment: a review. Rev Environ Sci Bio Technol 16(4):667–693. https://doi.org/10.1007/S11157-017-9445-Y

Chen D, Zeng Z, Zeng Y, Zhang F, Wang M (2016) Removal of methylene blue and mechanism on magnetic γ-Fe$_2$O$_3$/SiO$_2$ nanocomposite from aqueous solution. Water Resour Ind 15:1–13. https://doi.org/10.1016/J.WRI.2016.05.003

Chowdhury S, Mishra R, Kushwaha P, Saha P (2012) Removal of safranin from aqueous solutions by NaOH-treated rice husk: thermodynamics, kinetics and isosteric heat of adsorption. Asia-Pacific J Chem Eng 7:236–249. https://doi.org/10.1002/APJ.525

Daneshvar E, Vazirzadeh A, Niazi A, Kousha M, Naushad M, Bhatnagar A (2017) Desorption of methylene blue dye from brown macroalga: effects of operating parameters, isotherm study and kinetic modeling. J Clean Prod 152:443–453. https://doi.org/10.1016/J.JCLEPRO.2017.03.119

Dawood S, Sen TK, Phan C (2016) Adsorption removal of methylene blue (MB) dye from aqueous solution by bio-char prepared from eucalyptus sheathiana bark: kinetic, equilibrium, mechanism, thermodynamic and process design. New Pub Balaban 57:28964–28980. https://doi.org/10.1080/19443994.2016.1188732

Deng D, Lamssali M, Aryal N, Ofori-Boadu A, Jha MK, Samuel RE (2020) Textiles wastewater treatment technology: a review. Water Environ Res 92:1805–1810. https://doi.org/10.1002/WER.1437

Djenouhat M, Hamdaoui O, Chiha M, Samar MH (2008) Ultrasonication-assisted preparation of water-in-oil emulsions and application to the removal of cationic dyes from water by emulsion liquid membrane: part 2. Permeat Stripping Sep Purif Technol 63:231–238. https://doi.org/10.1016/J.SEPPUR.2008.05.005

Doğan M, Alkan M, Türkyilmaz A, Özdemir Y (2004) Kinetics and mechanism of removal of methylene blue by adsorption onto perlite. J Hazard Mater 109:141–148. https://doi.org/10.1016/J.JHAZMAT.2004.03.003

El-Deen RAS, Mohamed NY, Mahmoud AS (2022) Thermodynamic equilibrium kinetics of sewage sludge ash pellets for the removal of methylene blue (MB) from aqueous solutions. Key Eng Mater 921:161–172. https://doi.org/10.4028/P-VW0A4U

El-khatib AM, Elsafi M, Sayyed MI, Abbas MI, El-Khatib M (2021) Impact of micro and nano aluminium on the efficiency of photon detectors. Results Phys 30:104908. https://doi.org/10.1016/J.RINP.2021.104908

El-Sayed GO (2011) Removal of methylene blue and crystal violet from aqueous solutions by palm kernel fiber. Desalination 272:225–232. https://doi.org/10.1016/J.DESAL.2011.01.025

El-Shafei MM, Mahmoud AS, Mostafa MK, Peters RW (2016) Effects of entrapped nZVI in alginate polymer on BTEX removal [WWW Document]. Environ Div 2016–Core Program Area 2016 AIChE Annu Meet https://www.aiche.org/conferences/aiche-annual-meeting/2016/proceeding/paper/60b-effects-entrapped-nzvi-alginate-polymer-on-btex-removal Accessed 5 Aug 22

Elshayb OM, Nada AM, Sadek AH, Ismail SH, Shami A, Alharbi BM, Alhammad BA, Seleiman MF (2022) The integrative effects of biochar and ZnO nanoparticles for enhancing rice productivity and water use efficiency under irrigation deficit conditions. Plants 11(11):1416. https://doi.org/10.3390/PLANTS11111416

Elshfai MM, Hassan RG, Mahmoud AS (2022) Reduction of biological contaminants from municipal wastewater by encapsulated nZVI in alginate (Ag) polymer: reduction mechanism with artificial intelligence approach. Key Eng Mater 921:173–189. https://doi.org/10.4028/P-PK7PA4

Fan J, Guo Y, Wang J, Fan M (2009) Rapid decolorization of azo dye methyl orange in aqueous solution by nanoscale zerovalent iron particles. J Hazard Mater 166:904–910. https://doi.org/10.1016/J.JHAZMAT.2008.11.091

Fernandes AN, Almeida CAP, Debacher NA, Sierra MMDS (2010) Isotherm and thermodynamic data of adsorption of methylene blue from aqueous solution onto peat. J Mol Struct 982:62–65. https://doi.org/10.1016/J.MOLSTRUC.2010.08.006

Fil BA, Korkmaz M, Özmetin C (2014) An empirical model for adsorption thermodynamics of copper (II) from solutions onto illite clay-batch process design. J Chil Chem Soc 59:2686–2691. https://doi.org/10.4067/S0717-97072014000400012

Foo KY, Hameed BH (2012) An overview of dye removal via activated carbon adsorption process. New Pub Balaban 19:255–274. https://doi.org/10.5004/DWT.2010.1214

Gar Alalm M, Nasr M (2018) Artificial intelligence, regression model, and cost estimation for removal of chlorothalonil pesticide by activated carbon prepared from casuarina charcoal. Sustain Environ Res 28:101–110. https://doi.org/10.1016/J.SERJ.2018.01.003

Garg VK, Amita M, Kumar R, Gupta R (2004) Basic dye (methylene blue) removal from simulated wastewater by adsorption using Indian rosewood sawdust: a timber industry waste. Dye Pigment 63:243–250. https://doi.org/10.1016/J.DYEPIG.2004.03.005

Geçgel Ü, Özcan G, Gürpnar GÇ (2013) Removal of methylene blue from aqueous solution by activated carbon prepared from pea shells (Pisum sativum). J Chem. https://doi.org/10.1155/2013/614083

Ghasemi J, Asadpour S (2007) Thermodynamics' study of the adsorption process of methylene blue on activated carbon at different

ionic strengths. J Chem Thermodyn 39:967–971. https://doi.org/10.1016/J.JCT.2006.10.018

González-Gómez MA, Belderbos S, Yañez-Vilar S, Piñeiro Y, Cleeren F, Bormans G, Deroose CM, Gsell W, Himmelreich U, Rivas J (2019) Development of superparamagnetic nanoparticles coated with polyacrylic acid and aluminum hydroxide as an efficient contrast agent for multimodal imaging. Nanomater 9(11):1626. https://doi.org/10.3390/NANO9111626

Gouamid M, Ouahrani MR, Bensaci MB (2013) Adsorption equilibrium, kinetics and thermodynamics of methylene blue from aqueous solutions using date palm leaves. Energy Proced 36:898–907. https://doi.org/10.1016/J.EGYPRO.2013.07.103

Gulicovski JJ, Čerović LS, Milonjić SK (2008) Point of zero charge and isoelectric point of alumina. Mater Manuf Process 23:615–619. https://doi.org/10.1080/10426910802160668

Hamdy A (2021) Experimental study of the relationship between dissolved iron, turbidity, and removal of Cu(II) ion from aqueous solutions using zero-valent iron nanoparticles. Arab J Sci Eng 46:5543–5565. https://doi.org/10.1007/S13369-020-05079-0/FIGURES/5

Hamdy A, Mostafa MK, Nasr M (2018) Zero-valent iron nanoparticles for methylene blue removal from aqueous solutions and textile wastewater treatment, with cost estimation. Water Sci Technol 78:367–378. https://doi.org/10.2166/WST.2018.306

Hamdy A, Mostafa MK, Nasr M (2019a) Regression analysis and artificial intelligence for removal of methylene blue from aqueous solutions using nanoscale zero-valent iron. Int J Environ Sci Technol 16:357–372. https://doi.org/10.1007/S13762-018-1677-Z/TABLES/4

Hamdy A, Mostafa MK, Nasr M (2019b) Techno-economic estimation of electroplating wastewater treatment using zero-valent iron nanoparticles: batch optimization, continuous feed, and scaling up studies. Environ Sci Pollut Res Int 26:25372–25385. https://doi.org/10.1007/S11356-019-05850-3

Hamdy A, Ismail SH, Ebnalwaled AA, Mohamed GG (2021) Characterization of superparamagnetic/monodisperse PEG-coated magnetite nanoparticles sonochemically prepared from the hematite ore for Cd(II) removal from aqueous solutions. J Inorg Organomet Polym Mater 31:397–414. https://doi.org/10.1007/S10904-020-01741-0/TABLES/7

Hassan MM, Carr CM (2018) A critical review on recent advancements of the removal of reactive dyes from dyehouse effluent by ion-exchange adsorbents. Chemosphere 209:201–219. https://doi.org/10.1016/J.CHEMOSPHERE.2018.06.043

Ho YS, McKay G (1999) Pseudo-second order model for sorption processes. Process Biochem 34:451–465. https://doi.org/10.1016/S0032-9592(98)00112-5

Hu XJ, Wang JS, Liu YG, Li X, Zeng GM, Bao ZL, Zeng XX, Chen AW, Long F (2011) Adsorption of chromium (VI) by ethylenediamine-modified cross-linked magnetic chitosan resin: Isotherms, kinetics and thermodynamics. J Hazard Mater 185:306–314. https://doi.org/10.1016/J.JHAZMAT.2010.09.034

Huang C, Chen X, Xue Z, Wang T (2020) Effect of structure: a new insight into nanoparticle assemblies from inanimate to animate. Sci Adv. https://doi.org/10.1126/SCIADV.ABA1321/ASSET/07B0DD3D-CDA2-4205-B67F-FF94DD221A6C/ASSETS/GRAPHIC/ABA1321-F8.JPEG

Ileri B, Dogu I (2022) Sono–degradation of reactive blue 19 in aqueous solution and synthetic textile industry wastewater by nanoscale zero–valent aluminum. J Environ Manage 303:114200. https://doi.org/10.1016/J.JENVMAN.2021.114200

Imran M, Crowley DE, Khalid A, Hussain S, Mumtaz MW, Arshad M (2015) Microbial biotechnology for decolorization of textile wastewaters. Rev Environ Sci Biotechnol 14:73–92. https://doi.org/10.1007/S11157-014-9344-4/TABLES/3

Ismail B, Hussain ST, Akram S (2013) Adsorption of methylene blue onto spinel magnesium aluminate nanoparticles: adsorption isotherms, kinetic and thermodynamic studies. Chem Eng J 219:395–402. https://doi.org/10.1016/J.CEJ.2013.01.034

Karthikeyan T, Rajgopal S, Miranda LR (2005) Chromium(VI) adsorption from aqueous solution by hevea brasilinesis sawdust activated carbon. J Hazard Mater 124:192–199. https://doi.org/10.1016/J.JHAZMAT.2005.05.003

Kavitha D, Namasivayam C (2007) Experimental and kinetic studies on methylene blue adsorption by coir pith carbon. Bioresour Technol 98:14–21. https://doi.org/10.1016/J.BIORTECH.2005.12.008

Khosravi M, Arabi S (2016) Application of response surface methodology (RSM) for the removal of methylene blue dye from water by nano zero-valent iron (NZVI). Water Sci Technol 74:343–352. https://doi.org/10.2166/WST.2016.122

Kuo CY, Wu CH, Wu JY (2008) Adsorption of direct dyes from aqueous solutions by carbon nanotubes: determination of equilibrium, kinetics and thermodynamics parameters. J Colloid Interface Sci 327:308–315. https://doi.org/10.1016/J.JCIS.2008.08.038

Langmuir I, Waugh DF (2002) Pressure-soluble and pressure-displaceable components of monolayers of native and denatured proteins. J Am Chem Soc 62:2771–2793. https://doi.org/10.1021/JA01867A046

Lellis B, Fávaro-Polonio CZ, Pamphile JA, Polonio JC (2019) Effects of textile dyes on health and the environment and bioremediation potential of living organisms. Biotechnol Res Innov 3:275–290. https://doi.org/10.1016/J.BIORI.2019.09.001

Li X, Zhang M, Liu Y, Li X, Liu Y, Hua R, He C (2013a) Removal of U(VI) in aqueous solution by nanoscale zero-valent iron(nZVI). Water Qual Expo Heal 51(5):31–40. https://doi.org/10.1007/S12403-013-0084-4

Li Y, Du Q, Liu T, Peng X, Wang J, Sun J, Wang Y, Wu S, Wang Z, Xia Y, Xia L (2013b) Comparative study of methylene blue dye adsorption onto activated carbon, graphene oxide, and carbon nanotubes. Chem Eng Res Des 91:361–368. https://doi.org/10.1016/J.CHERD.2012.07.007

Liu L, Fan S, Li Y (2018) Removal behavior of methylene blue from aqueous solution by tea waste: kinetics, isotherms and mechanism. Int J Environ Res Public Health. https://doi.org/10.3390/IJERPH15071321

Lozhkomoev AS, Rodkevich NG, Vorozhtsov AB, Lerner MI (2020) Oxidation and oxidation products of encapsulated aluminum nanopowders. J Nanoparticle Res 22:1–13. https://doi.org/10.1007/S11051-019-4748-2/FIGURES/11

Mahmoud AS (2022) Effect of nano bentonite on direct yellow 50 dye removal; adsorption isotherm, kinetic analysis, and thermodynamic behavior. Prog React Kinet Mech. https://doi.org/10.1177/14686783221090377

Mahmoud MS, Mahmoud AS (2021) Wastewater treatment using nano bimetallic iron/copper, adsorption isotherm, kinetic studies, and artificial intelligence neural networks. Emergent Mater 4:1455–1463. https://doi.org/10.1007/S42247-021-00253-Y/TABLES/2

Mahmoud MS, Mahmoud AS (2022) Treatment of chromium from tannery wastewater using nano-bio polymer complex. Key Eng Mater 921:191–203. https://doi.org/10.4028/P-G6WMW4

Mahmoud AS, Mostafa MK, Abdel-Gawad SA (2018a) Artificial intelligence for the removal of benzene, toluene, ethyl benzene and xylene (BTEX) from aqueous solutions using iron nanoparticles. Water Supply 18:1650–1663. https://doi.org/10.2166/WS.2017.225

Mahmoud AS, Mostafa MK, Nasr M (2018b) Regression model, artificial intelligence, and cost estimation for phosphate adsorption using encapsulated nanoscale zero-valent iron. Sep Sci Technol 54:13–26

Mahmoud AS, Farag RS, Elshfai MM, Mohamed LA, Ragheb SM (2019) Nano zero-valent aluminum (nZVAl) preparation,

characterization, and application for the removal of soluble organic matter with artificial intelligence, isotherm study, and kinetic analysis. Air Soil Water Res. https://doi.org/10.1177/1178622119878707

Mahmoud AS, Farag RS, Elshfai MM (2020) Reduction of organic matter from municipal wastewater at low cost using green synthesis nano iron extracted from black tea: artificial intelligence with regression analysis. Egypt J Pet 29:9–20. https://doi.org/10.1016/J.EJPE.2019.09.001

Mahmoud AS, Mohamed NY, Mostafa MK, Mahmoud MS (2021b) Effective chromium adsorption from aqueous solutions and tannery wastewater using bimetallic Fe/Cu nanoparticles: response surface methodology and artificial neural network. Air Soil Water Res. https://doi.org/10.1177/11786221211028162

Mahmoud AS, Mostafa MK, Peters RW (2021c) A prototype of textile wastewater treatment using coagulation and adsorption by Fe/Cu nanoparticles: Techno-economic and scaling-up studies. Nanomater Nanotechnol. https://doi.org/10.1177/18479804211041181

Mahmoud MS, Mahmoud AS, El-Said MA, Mostafa MK (2021d) Comparison of aluminum and iron nanoparticles for chromium removal from aqueous solutions and tannery wastewater, empirical modeling and prediction. Emergent Mater 1:1–16. https://doi.org/10.1007/S42247-021-00320-4/TABLES/5

Mahmoud AS, Mahmoud MS, Yousri N, Mostafa MK (2022) Advanced wastewater treatment by using entrapped nZVI into alginate (Ag) biopolymer: adsorption isotherm, kinetic models, and statistical analysis. Key Eng Mater 921:147–160. https://doi.org/10.4028/P-XYGKON

Mahmoud AS, Saryel-Deen RA, Mostafa MK (2017a) Artificial intelligence for organochlorine pesticides removal from aqueous solutions using entrapped nzvi in alginate biopolymer. In: Environmental division 2017a–core programming area at the 2017a AIChE annual meeting pp. 420–427

Mahmoud AS, SaryEl-deen RA, Mostafa MK, Peters RW (2017b) (655d) Artificial intelligence for organochlorine pesticides removal from aqueous solutions using entrapped nzvi in alginate biopolymer [WWW Document]. 2017b AIChE Annu Meet https://www.aiche.org/conferences/aiche-annual-meeting/2017b/proceeding/paper/655d-artificial-intelligence-organochlorine-pesticides-removal-aqueous-solutions-using-entrapped accessed 5 Aug 22

Mahmoud AS, Mahmoud MS, Ahmed MN, Peters RW, Mostafa MK, (2021a) (423f) Effective adsorption of chromium from tannery wastewater using green synthesis nano-zero valent iron (GT-nZVI) [WWW Document]. 2021a AIChE Annu. Meet https://www.aiche.org/academy/conferences/aiche-annual-meeting/2021a/proceeding/paper/423f-effective-adsorption-chromium-tannery-wastewater-using-green-synthesis-nano-zero-valent-iron-gt accessed 5 Aug 22

Mohammadzadeh Kakhki R, Mohammadpoor M, Faridi R, Bahadori M (2020) The development of an artificial neural network–genetic algorithm model (ANN-GA) for the adsorption and photocatalysis of methylene blue on a novel sulfur–nitrogen co-doped Fe_2O_3 nanostructure surface. RSC Adv 10:5951–5960. https://doi.org/10.1039/C9RA10349J

Mostafa MK, Mahmoud AS, SaryEl-Deen RA, Peters RW (2017) Application of entrapped nano zero valent iron into cellulose acetate membranes for domestic wastewater treatment [WWW Document]. Environ Asp Appl Implic Nanomater Nanotechnol 2017–Top Conf 2017 AIChE Annu Meet https://www.aiche.org/conferences/aiche-annual-meeting/2017/proceeding/paper/549e-application-entrapped-nano-zero-valent-iron-cellulose-acetate-membranes-domestic-wastewater accessed 5 Aug 22

Mostafa MK, Mahmoud AS, Kamar MT, Elshfai MM, Moussa M, Peters RW, (2021) (48d) Effective municipal wastewater treatment at low-cost using coagulation/precipitation followed by nano-disinfection [WWW Document]. 2021 AIChE Annu Meet https://www.aiche.org/academy/conferences/aiche-annual-meeting/2021/proceeding/paper/48d-effective-municipal-wastewater-treatment-low-cost-using-coagulationprecipitation-followed-nano accessed 5 Aug 22

Mouni L, Belkhiri L, Bollinger JC, Bouzaza A, Assadi A, Tirri A, Dahmoune F, Madani K, Remini H (2018) Removal of methylene blue from aqueous solutions by adsorption on kaolin: kinetic and equilibrium studies. Appl Clay Sci 153:38–45. https://doi.org/10.1016/J.CLAY.2017.11.034

Nidheesh PV, Khatri J, Anantha Singh TS, Gandhimathi R, Ramesh ST (2018) Review of zero-valent aluminium based water and wastewater treatment methods. Chemosphere 200:621–631. https://doi.org/10.1016/J.CHEMOSPHERE.2018.02.155

Önal Y, Akmil-Başar C, Eren D, Sarici-Özdemir Ç, Depci T (2006) Adsorption kinetics of malachite green onto activated carbon prepared from Tunçbilek lignite. J Hazard Mater 128:150–157. https://doi.org/10.1016/J.JHAZMAT.2005.07.055

Oprčkal P, Mladenovič A, Vidmar J, Mauko Pranjić A, Milačič R, Ščančar J (2017) Critical evaluation of the use of different nanoscale zero-valent iron particles for the treatment of effluent water from a small biological wastewater treatment plant. Chem Eng J 321:20–30. https://doi.org/10.1016/J.CEJ.2017.03.104

Pathania D, Sharma S, Singh P (2017) Removal of methylene blue by adsorption onto activated carbon developed from Ficus carica bast. Arab J Chem 10:S1445–S1451. https://doi.org/10.1016/J.ARABJC.2013.04.021

Peng T, Guo XH, Yang Y, Gai WZ, Deng ZY (2022) Soaked Al powder for efficient reduction of hexavalent chromium in neutral solution. J Clean Prod 365:132901. https://doi.org/10.1016/J.JCLEPRO.2022.132901

Petala E, Dimos K, Douvalis A, Bakas T, Tucek J, Zbořil R, Karakassides MA (2013) Nanoscale zero-valent iron supported on mesoporous silica: characterization and reactivity for Cr(VI) removal from aqueous solution. J Hazard Mater 261:295–306. https://doi.org/10.1016/J.JHAZMAT.2013.07.046

Rahimi N, Pax RA, Gray EM (2016) Review of functional titanium oxides. I: TiO_2 and its modifications. Prog Solid State Chem 44(3):1–55. https://doi.org/10.1016/j.progsolidstchem.2016.07.002

Raman CD, Kanmani S (2016) Textile dye degradation using nano zero valent iron: a review. J Environ Manage 177:341–355. https://doi.org/10.1016/J.JENVMAN.2016.04.034

Ratnam MV, Murugesan MP, Komarabathina S, Samraj S, Abdulkadir M, Kalifa MA (2022) Methylene blue adsorption BY UV-treated graphene oxide nanoparticles (UV/n-GO): modeling and optimization using response surface methodology and artificial neural networks. Int J Chem Eng 2022:1–13. https://doi.org/10.1155/2022/5759394

Sadegh H, Ali GAM, Gupta VK, Makhlouf ASH, Shahryari-ghoshekandi R, Nadagouda MN, Sillanpää M, Megiel E (2017) The role of nanomaterials as effective adsorbents and their applications in wastewater treatment. J Nanostruct Chem 71(7):1–14. https://doi.org/10.1007/S40097-017-0219-4

Sadek AH, Asker MS, Abdelhamid SA (2021) Bacteriostatic impact of nanoscale zero-valent iron against pathogenic bacteria in the municipal wastewater. Biologia (bratisl) 76:2785–2809. https://doi.org/10.1007/S11756-021-00814-W/TABLES/10

Sadek AHSE-D, Mostafa M (2019) Preparation of zerovalent aluminium nanoparticles at room temperature and uses thereof | the lens [WWW Document]. WO 2019/057262 A1 https://www.lens.org/lens/patent/168-272-206-829-327/frontpage accessed 28 Jan 22

Saha P (2010) Assessment on the removal of methylene blue dye using tamarind fruit shell as biosorbent. Water Air Soil Pollut 213:287–299. https://doi.org/10.1007/S11270-010-0384-2/FIGURES/8

Sahu RK, Hiremath SS, Manivannan PV, Singaperumal M (2014) An innovative approach for generation of aluminium nanoparticles using micro electrical discharge machining. Proced Mater Sci 5:1205–1213. https://doi.org/10.1016/J.MSPRO.2014.07.424

Salimi F, Rahimi H, Karami C (2019) Removal of methylene blue from water solution by modified nanogoethite by Cu. Desalin Water Treat. https://doi.org/10.5004/dwt.2019.22922

SaryEl-deen RA, Mahmoud AS, Mahmoud MS, Mostafa MK, Peters RW (2017) Adsorption and kinetic studies of using entrapped sewage sludge ash in the removal of chemical oxygen demand from domestic wastewater, with artificial intelligence approach [WWW Document]. Poster Sess 2017–Core Program Area 2017 AIChE Annu Meet https://www.aiche.org/conferences/aiche-annual-meeting/2017/proceeding/paper/583aa-adsorption-and-kinetic-studies-using-entrapped-sewage-sludge-ash-removal-chemical-oxygen accessed 5 Aug 22

Satapanajaru T, Chompuchan C, Suntornchot P, Pengthamkeerati P (2011) Enhancing decolorization of reactive black 5 and reactive red 198 during nano zerovalent iron treatment. Desalination 266:218–230. https://doi.org/10.1016/J.DESAL.2010.08.030

Senthilkumaar S, Varadarajan PR, Porkodi K, Subbhuraam CV (2005) Adsorption of methylene blue onto jute fiber carbon: kinetics and equilibrium studies. J Colloid Interface Sci 284:78–82. https://doi.org/10.1016/J.JCIS.2004.09.027

Shih YH, Hsu CY, Su YF (2011) Reduction of hexachlorobenzene by nanoscale zero-valent iron: kinetics, pH effect, and degradation mechanism. Sep Purif Technol 76:268–274. https://doi.org/10.1016/J.SEPPUR.2010.10.015

Smith DK, Unruh DK, Wu CC, Pantoya ML (2017) Replacing the Al_2O_3 shell on Al particles with an oxidizing salt, aluminum iodate hexahydrate. part I: reactivity. J Phys Chem C 121:23184–23191. https://doi.org/10.1021/ACS.JPCC.7B05803/ASSET/IMAGES/MEDIUM/JP-2017-05803J_0009.GIF

Soldatkina L, Yanar M (2021) Equilibrium, kinetic, and thermodynamic studies of cationic dyes adsorption on corn stalks modified by citric acid. Coll Interfaces 5(4):52. https://doi.org/10.3390/COLLOIDS5040052

Sun Z, Li C, Wu D (2010) Removal of methylene blue from aqueous solution by adsorption onto zeolite synthesized from coal fly ash and its thermal regeneration. J Chem Technol Biotechnol 85:845–850. https://doi.org/10.1002/JCTB.2377

Suteu D, Malutan T (2013) Industrial cellolignin wastes as adsorbent for removal of methylene blue dye from aqueous solutions. BioResources. https://doi.org/10.15376/biores.8.1.427-446

Tang R, Dai C, Li C, Liu W, Gao S, Wang C (2017) Removal of methylene blue from aqueous solution using agricultural residue walnut shell: equilibrium, kinetic, and thermodynamic studies. J Chem. https://doi.org/10.1155/2017/8404965

Velusamy S, Roy A, Sundaram S, Kumar Mallick T (2021) A review on heavy metal ions and containing dyes removal through graphene oxide-based adsorption strategies for textile wastewater treatment. Chem Rec 21:1570–1610. https://doi.org/10.1002/TCR.202000153

Wang T, Jin X, Chen Z, Megharaj M, Naidu R (2014) Green synthesis of Fe nanoparticles using eucalyptus leaf extracts for treatment of eutrophic wastewater. Sci Total Environ 466–467:210–213. https://doi.org/10.1016/J.SCITOTENV.2013.07.022

Wang JH, Mahmoud MS, Mahmoud AS (2021) Integrated efficiency of using nanocellulose-nano zero valent iron composite in water treatment. BioResources. https://doi.org/10.15376/biores.17.1.975-992

Weber WJ Jr, Morris JC (1963) Kinetics of adsorption on carbon from solution. J Sanit Eng Div 89:31–59. https://doi.org/10.1061/JSEDAI.0000430

Wei X, Wang Y, Feng Y, Xie X, Li X, Yang S (2019a) Different adsorption-degradation behavior of methylene blue and Congo red in nanoceria/H2O2 system under alkaline conditions. Sci Reports. https://doi.org/10.1038/s41598-018-36794-2

Wei X, Wang Y, Feng Y, Xie X, Li X, Yang S (2019b) Different adsorption-degradation behavior of methylene blue and Congo red in nanoceria/H2O2 system under alkaline conditions. Sci Reports. https://doi.org/10.1038/s41598-018-36794-2

Wu YC, Wei YH, Wu HS (2021) Adsorption and desorption behavior of ectoine using dowex® HCR-S ion-exchange resin. Process 9(11):2068. https://doi.org/10.3390/PR9112068

Xia Y, Yao Q, Zhang W, Zhang Y, Zhao M (2019) Comparative adsorption of methylene blue by magnetic baker's yeast and EDTAD-modified magnetic baker's yeast: equilibrium and kinetic study. Arab J Chem 12:2448–2456. https://doi.org/10.1016/J.ARABJC.2015.03.010

Xie S, Yang Y, Gai WZ, Deng ZY (2020) Oxide modified aluminum for removal of methyl orange and methyl blue in aqueous solution. RSC Adv 11:867–875. https://doi.org/10.1039/D0RA09048D

Yang ST, Chen S, Chang Y, Cao A, Liu Y, Wang H (2011) Removal of methylene blue from aqueous solution by graphene oxide. J Colloid Interface Sci 359:24–29. https://doi.org/10.1016/J.JCIS.2011.02.064

Zhang G, Wo R, Sun Z, Hao G, Liu G, Zhang Y, Guo H, Jiang W (2021) Effective magnetic MOFs adsorbent for the removal of bisphenol a, tetracycline, congo red and methylene blue pollutions. Nanomater 11(8):1917. https://doi.org/10.3390/NANO11081917